NPL Report DEPC-MPR 007

Determination of Material Properties and Parameters Required for the Simulation of Impact Performance of Plastics Using Finite Element Analysis

G Dean and R Mera

July 2004

NPL Report DEPC-MPR 007

July 2004

Determination of Material Properties and Parameters Required for the Simulation of Impact Performance of Plastics Using Finite Element Analysis

G Dean and R Mera
Engineering and Process Control Division
National Physical Laboratory
Teddington, Middlesex TW11 0LW, UK

SUMMARY

Measurement methods are briefly described for determining true stress/true strain curves for ductile plastics under tension, shear and compression. Measurements have been made on a talc filled, rubber-toughened propylene-ethylene copolymer used for the manufacture of motor vehicle interior door trim. Results are analysed to determine the properties and parameters required by selected elastic-plastic models for the simulation of impact performance using finite element methods. For this purpose, measurements under tension are required out to large strains and over a wide range of strain rate which includes very high rates (~ 1000 s^{-1}) associated with impact events. Measurements at large strains are achieved using a non-standard test specimen shape. The determination of properties at high strain rates is achieved by modelling measurements at low and moderate strain rates and calculating the behaviour at high strain rates by extrapolation.

Measurements of stress/strain curves under tension, shear and compression and of Poisson's ratio with strain are used to derive parameters for the von Mises and linear Drucker-Prager models and for a new model that takes account of the influence of cavitation on plastic deformation. Limitations in the applicability of the first two models for describing the deformation behaviour of the copolymer are demonstrated. The results of measurements made on injection moulded specimens of the copolymer and specimens cut from a component moulding are compared.

The implications of differences in these results on the determination of model parameters are discussed.

ISSN 1744-0270

National Physical Laboratory
Teddington, Middlesex, UK, TW11 0LW

We gratefully acknowledge the financial support of the UK Department of Trade and Industry (National Measurement System Policy Unit)

Approved on behalf of the Managing Director,NPL,
by Dr M G Cain, Knowledge Leader, Materials Processing Team
authorised by Director, Engineering and Process Control Division

CONTENTS

1 INTRODUCTION

This project is comprised of the following 3 main task areas:

1. tests over a range of test speeds on regions cut from mouldings of an interior door trim panel supplied by Land Rover.

2. simulation of the deformation behaviour of these regions using finite element analyses with different elastic-plastic models for comparison with the above measurements. The models being used are based on the von Mises and linear Drucker-Prager yield criteria and a new model that takes account of the influence of the nucleation of cavities in the polymer on yield behaviour.

3. determination of the properties and parameters required by these models from measurements on ISO standard injection moulded specimens and specimens cut from door trim mouldings.

This report describes the test methods, results and data analysis related to the task area 3 above.

2 MATERIAL

The polymer investigated in this study is a rubber-toughened propylene-ethylene copolymer containing about 17% by weight of filler which is mainly talc. The material was produced by Dow Plastics with the identification code DTF 1600.00S. Test specimens were obtained from two sources. Dow supplied injection moulded specimens in the form of standard tensile bars (1) and 80 mm square plates. Also, interior door trim panels were supplied by Intier who manufacture these components by extrusion compression moulding for Land Rover. Test specimens of suitable geometry were machined from appropriate regions of these panels.

The results of tensile and shear tests on injection moulded specimens and specimens cut from the door trim revealed small differences in properties. Sample material from both sources was sent to RAPRA to carry out studies of the structure of the polymer.

The main difference in the structure is likely to arise from the nature and level of molecular orientation in each source arising from different processing conditions during moulding. RAPRA were however unable to measure molecular orientation because of the high levels of filler present. The main structural differences that they were able to detect are

- a higher content of crystalline polyethylene in the injection moulded specimen revealed by the prominence of the peak at 120 °C in a DSC scan.
- a slightly higher and wider molecular weight distribution for the injection moulded specimen revealed by gel-permeation chromatography.

It is not clear whether the results of these measurements arise through the use of different batches or different grades of the polymer or to what extent they can be attributed solely to different processing conditions. In addition, the probable differences in the nature and level of molecular orientation in the two sources of specimens raises some concern with the suitability of results on standard injection moulded test specimens for accurate design.

3 TEST METHODS

3.1 GENERAL

The data requirements for simulating the impact performance of a component using finite element methods depend on the choice of materials model used to describe the deformation behaviour of the polymer as well as any approximating assumptions, for example, associated with the dependence of properties on strain rate. For the determination of all the parameters in the cavitation model, measurements of stress/strain behaviour are needed in tension, shear and compression. Results for the variation of Poisson’s ratio with tensile strain are also needed. Although all of these measurements are not needed for the determination of parameters for other models considered here, it is informative to use the results to assess the

applicability of these models and the nature and magnitude of errors associated with their use.

In a previous project, test methods and procedures for the analysis of test data have been developed to determine

- the variation of tensile modulus with strain rate
- true stress/true strain curves in tension out to large strains
- the variation of tensile stress/strain behaviour with strain rate
- stress/strain curves in shear
- stress/strain behaviour under uniaxial compression.

Brief descriptions of the test methods will be given in the remainder of this section together with references to where more detailed information can be found. Procedures for determining the rate dependence of properties and the parameters required by different models are described in section 6.

3.2 TENSILE TESTS

3.2.1 At low strains

Engineering stress/strain curves in tension and Poisson's ratio were measured using the procedure defined by an ISO standard (1). This method is suitable for test speeds up to 1 mm/s (strain rate ~ 0.01 s^{-1}) but for higher speeds an alternative specimen geometry is preferable (see section 3.2.2). This method is also only suitable for the measurement of strain up to the peak in the stress/strain curve. At higher strains, the strain distribution in the parallel portion of the specimen is no longer uniform because of the onset of strain localisation. An alternative specimen geometry is then employed as described in the next section.

3.2.2 At high strains

Figure 1 shows results of tensile stress against tensile strain measurements on a single specimen of a rubber-toughened polypropylene. The specimen geometry and dimensions were the same as the ISO tensile specimen (1). Simultaneous strain measurements were made using a video extensometer in three separate regions of length 10 mm near the centre of the specimen. The results illustrate the distribution of strain that can occur in specimens of this geometry at strains above that corresponding to the peak in stress. The extent of the strain localisation depends on the flow behaviour of the polymer and hence the test temperature and speed. In extreme situations, the localisation is clearly visible through necking but for many materials the extent of the non-uniformity in strain is less extreme and less apparent.

In order to obtain more meaningful measurements of strain, and, in particular, of strain at failure, an alternative specimen geometry has been chosen that is illustrated in figure 2. The waisted region is defined by a constant radius that locates the maximum stress, and hence onset of flow, at the centre of the specimen. The specimen can be conveniently machined from the central region of the ISO tensile specimen. Finite element analyses have been used (2) to calculate stress and strain distributions in the specimen under an applied load that was sufficient to cause plastic flow in the central region. Calculated distributions depended on the hardening behaviour of the polymer but revealed an essentially uniform stress and strain over a length of between 3 and 5 mm in the specimen centre. Extensometers (contacting and video) have therefore been used with a gauge length of 4 mm for the measurement of strain for the results reported here. Since this leads to significant uncertainties in the measurement of small strains (< 0.02), this specimen is used only for the determination of properties at moderate and high strains.

This specimen is also used for the measurement of Poisson's ratio at moderate and high strains through simultaneous measurements of lateral strain in the width direction at the specimen centre and axial strain. This is believed to give more reliable results than the use of the standard specimen because of the greater precision in the determination of the axial strain at the location of the transverse strain measurement. It is worth noting however, that the finite element calculations reveal a slightly smaller transverse strain in the width direction at the specimen centre than in the thickness direction. This arises presumably because of some

small constraint to free lateral contraction in the width direction owing to the presence of the waist profile. For the Poisson's ratio results reported here no attempt has been made to correct for this source of error.

3.2.3 At high strain rates

The small waisted specimen geometry shown in figure 2 can be used for the determination of tensile behaviour over a wide range of strain rate. For a given test speed, the strain rate in the central region of the specimen is significantly higher than obtained with the standard ISO specimen. Light-weight, contacting extensometers were used for axial strain measurement and were satisfactory at test speeds up to 100 mm/s where the strain rate in the gauge region is typically 10 s^{-1}. At this speed, errors in force measurement arising from resonances in the test assembly and wave effects in the specimen are generally negligible. The determination of properties at higher strain rates is achieved by modelling and extrapolation as described in section 6.5.

3.3 SHEAR TESTS

Shear measurements were carried out using a version of the test first proposed by Arcan et al (3). The test specimen geometry and loading stages are shown in figure 3. The distance between the notches in the specimen is 10 mm and the notch radius is 1.5 mm. Shear strains were measured using a purpose-built extensometer that measures the relative displacement of points separated by a distance of 3 mm at the centre of the specimen. In the calculation of shear stresses and strains, small corrections were applied for the non-uniform shear stress between the notches and for a contribution from bending to measured displacements.

3.4 COMPRESSION TESTS

Compression measurements were made on specimens with dimensions 10 mm × 10 mm cut from the gauge region of injection moulded, standard tensile specimens. End faces were machined smooth and accurately parallel. Specimens were loaded between parallel platens the faces of which were lubricated with oil. Because of the square geometry of the specimens, they could be loaded in the direction of the length of the original specimen or transverse to this direction to reveal any anisotropy in behaviour arising from molecular orientation during

injection moulding. Extensometers were used to measure changes in the platen separation, and nominal strains were derived from the original specimen length.

4 RESULTS

4.1 RESULTS FOR INJECTION MOULDED SPECIMENS

Figure 4 shows the tensile behaviour of the polymer measured on a specimen of the waisted geometry (figure 2) that was machined from the central region of a standard, injection moulded specimen. True values of stress σ were calculated from each engineering value of stress σ' and strain ε' and Poisson's ratio ν' using

$$\sigma = \frac{\sigma'}{(1 - \nu'\varepsilon')^2} \tag{1}$$

True values of strain, ε, were obtained using

$$\varepsilon = \ln(1 + \varepsilon') \tag{2}$$

Engineering values for Poisson's ratio are shown in figure 4 but true values for Poisson's ratio, ν, can be calculated from measured transverse strains, ε'_t, using

$$\nu = -\frac{\ln(1 + \varepsilon'_t)}{\ln(1 + \varepsilon')} \tag{3}$$

where ε'_t is negative. The progressive decrease in Poisson's ratio with strain observed in figure 4 arises because of the nucleation of cavities in the polymer under stress states with a significant hydrostatic component (see section 5.4). Poisson's ratio under a uniaxial compressive stress is essentially constant with strain.

Figure 5 compares stress/strain curves measured under tension, shear and compression at the same effective plastic strain rate of 0.01 s^{-1} (see section 6.4). The tensile curve was measured

using a standard, injection moulded specimen (section 3.2.1) to improve the precision of low-strain measurements. Tensile stresses are true values obtained using the Poisson's ratio data in figure 4. Compressive stresses are true values obtained using a constant value for Poisson's ratio of 0.4. The compressive curves were measured on specimens orientated along and transverse to the axis of the injection moulded specimen. Since this axis coincides with the direction of flow of the melt into the mould, the compression results indicate that the mechanical properties of the injection moulded specimen are anisotropic presumably as a result of molecular orientation. The shear results were obtained from a different injection moulded specimen. Since the melt flow conditions for this specimen are different from those associated with the preparation of the tensile specimen, the structure and hence properties of these specimens are likely to be different. Any attempt, therefore, to use these results to derive values for the parameters in materials models used by finite element systems will give uncertain errors in derived values. The results suggest that a more reliable approach to the determination of material properties and model parameters is to carry out tests on specimens cut from the door trim moulding.

4.2 RESULTS FOR SPECIMENS CUT FROM DOOR TRIM

Tensile specimens of both the ISO and the waisted specimen geometries were cut from regions of the door trim that will be used for impact tests at a later stage of the project. Shear specimens were cut from areas nearby. Compression tests could not be undertaken because the moulding thickness of 2 mm was too small to permit compressive deformation to suitable strains without buckling. Figure 6 compares tensile curves measured on three specimens cut from the trim moulding having the ISO geometry with the ISO injection moulded specimen data shown in figure 5. The result for specimen M1S1 illustrates the problem with strain measurement near the stress maximum arising from strain localisation in the specimen (see section 3.2.2). It is apparent that the tensile modulus of the door trim is higher than the injection moulded material. It is unlikely that this results from a higher level of molecular orientation in the door trim since the orientation is already high in the injection moulded specimen. It may be caused by small differences in the grade of polymer as implied by some of the results from structural evaluations described in section 2. Also, there are differences in the hardening behaviour of the two sources of material. This again could be caused by small differences in the grade of the polymer or by differences in crystallinity or molecular

orientation produced by the moulding methods that lead to different rates of nucleation of cavities under a tensile stress (see section 5.4).

Figure 7 compares shear curves for specimens cut from the door trim and from an injection moulded plate. The results are consistent with tensile data, showing increases in both modulus and flow stress with the door trim material.

5 ELASTIC-PLASTIC MODELS

5.1 GENERAL

Elastic-plastic models are used by finite element methods to describe large strain, non-linear behaviour when this is caused by yielding and flow. With these models, behaviour at low strains is taken to be linear elastic and characterised by two materials parameters which are commonly the Young's modulus E and the elastic Poisson's ration ν^e. The onset of non-linearity in a stress/strain curve is attributed to plastic deformation and occurs at a stress level regarded as the first yield stress. The subsequent increase in stress with strain is associated with the effects of strain hardening. In this non-linear region, the total strain ε is considered to be the sum of an elastic component ε^e and a plastic component ε^p as shown schematically in figure 8, thus

$$\varepsilon = \varepsilon^e + \varepsilon^p \tag{4}$$

Plastic strain hardening is then characterised by a curve (hardening curve) describing the variation of yield stress with plastic strain. In the case of tensile hardening, equation (4) gives the tensile component of plastic strain ε_T^p as

$$\varepsilon_T^p = \varepsilon_T - \frac{\sigma_T}{E} \tag{5}$$

where ε_T is the total tensile strain. The tensile hardening curve is then the function $\sigma_T\left(\varepsilon_T^p\right)$.

Stress analysis calculations involve the use of a yield criterion and a flow law. Three yield criteria, each associated with a different elastic-plastic model, are introduced in this section together with the property data and parameters required by each model.

5.2 THE VON MISES MODEL

The simplest yield criterion takes the form

$$\sigma_e = \sigma_T \tag{6}$$

The criterion assumes that yielding is determined only by the magnitude of the effective shear stress σ_e which is related to principal components of the applied stress σ_1, σ_2 and σ_3 by

$$\sigma_e = \left\{\frac{1}{2}\left[(\sigma_1-\sigma_2)^2 + (\sigma_2-\sigma_3)^2 + (\sigma_3-\sigma_1)^2\right]\right\}^{1/2} \tag{7}$$

Since σ_T varies with plastic strain, equation (6) defines a state of yielding characterised by the tensile stress and the associated level of plastic strain.

5.3 THE LINEAR DRUCKER-PRAGER MODEL

Yielding in polymers is known to be sensitive to the hydrostatic component of stress as well as the shear component. Equation (6) can be extended to include hydrostatic stress sensitivity as follows

$$\sigma_e + \mu\sigma_m = \frac{(\mu+3)}{3}\,\sigma_T = \sigma_o \tag{8}$$

where σ_m is the hydrostatic component of stress given by

$$\sigma_m = \frac{1}{3}(\sigma_1 + \sigma_2 + \sigma_3) \tag{9}$$

The material parameter μ determines the sensitivity of yielding to hydrostatic stress.

The flow rule is used in elastic-plastic models for the determination of plastic strains through identification of a flow potential F. The most general form for the flow potential in the linear Drucker-Prager model is given by

$$F = \sigma_e + \mu' \sigma_m \tag{10}$$

The flow parameter μ' is a material property that differs from the value of μ in equation (8) if the polymer exhibits non-associated flow. It can be determined from measurement of the plastic component of Poisson's ration ν^p using the expression

$$\mu' = \frac{3(1-2\nu^p)}{2(1+\nu^p)} \tag{11}$$

5.4 THE CAVITATION MODEL

In certain polymers, the yield behaviour under tension is very different from that under compression or shear because of the nucleation of numerous small cavities in the polymer under stress. This is usually visible as stress whitening. In rubber-toughened plastics, the rubber particles are sites for cavity nucleation. In semi-crystalline polymers where the amorphous phase is rubbery, such as polyethylenes and polypropylenes at ambient temperatures, the sites of cavitation are the amorphous regions between crystallites. Cavity nucleation improves the toughness of the polymer by promoting localised but widespread shear yielding in the matrix material between cavities. It will therefore lower the yield stress under those stress states for which the hydrostatic stress component is sufficient to cause cavitation.

In the absence of cavitation, equation (8) is a satisfactory criterion for yielding. This equation is then modified to include the effects of cavitation as follows (4)

$$\frac{\sigma_e^2}{\sigma_M^2} - (q_1 f)^2 + 2q_1 f \cosh \frac{3\sigma_m}{2\sigma_M} = \left(1 - \frac{\mu\sigma_m}{\sigma_M}\right)^2 \tag{12}$$

Here f is the effective volume fraction of cavities which at small strains is zero but increases over some characteristic strain region associated with cavity nucleation. The term effective is used here since the actual volume of a cavity may be small but if the rubbery material surrounding the cavity offers negligible resistance to deformation then its effective size will be significantly larger. Neglecting cavity growth, the maximum value for f occurs when cavity nucleation is complete and is equal to the effective volume fraction v_C of the phase where cavities are assumed to nucleate. The value for v_C might be expected to vary with molecular orientation and crystallinity. The parameter q_1 has been introduced to account for the effect of void interactions on the stress distribution in the matrix between cavities.

σ_M is the effective yield stress of the matrix polymer between cavities and is equal to σ_o in the absence of cavities. As cavity nucleation proceeds and the rubbery regions become replaced by cavities, σ_M will increase with f. The relationship between σ_M and f will depend upon how the effective shear yield stress of the uncavitated polymer σ_o varies with the volume fraction of the cavitatable phase v_C. The results of experiments and model calculations on an unfilled propylene-ethylene copolymer suggest that this takes the form (5)

$$\sigma_o = \sigma_{MC} \exp\left[-(k v_C)\right] \tag{13}$$

where σ_{MC} is the effective shear yield stress of the rigid or uncavitated phase. The expression for σ_M is then given by

$$\sigma_M = \frac{\sigma_o}{\exp\left[-k v_C\right]} \exp\left[-k\frac{(v_C - f)}{(1-f)}\right] \tag{14}$$

From equation (8), $\sigma_o = \sqrt{3}\,\sigma_S$, where σ_S is a yield stress under shear, and is derived from experimental data obtained in shear and replaces σ_T as the basic hardening function for the polymer. The nucleation of a cavity is assumed to occur at some critical volumetric strain that varies with the size of the cavitatable region. For a distribution of sizes of these regions, the cavity nucleation should occur over a range of total volumetric strain ε_V.

Through comparisons with experimental data for a range of plastics, it has been shown that the increase in the volume fraction of nucleated cavities f with volumetric strain is given with satisfactory accuracy by the expressions (4)

$$\begin{aligned} f &= 0 \text{ for } \varepsilon_V \le \varepsilon_{1V} \\ f &= v_C \left\{ 1 - \exp\left[-\left(\frac{\varepsilon_V - \varepsilon_{1V}}{\varepsilon_{2V}} \right)^{\beta} \right] \right\} \text{ for } \varepsilon_V > \varepsilon_{1V} \end{aligned} \tag{15}$$

The parameters ε_{1V}, ε_{2V} and β determine the location and breadth of the volumetric strain range over which cavity nucleation occurs.

The results of axial and transverse strain measurements in the Land Rover polymer under uniaxial tension have revealed that flow in this polymer is non-associated. The flow potential is therefore, by analogy with equation (10)), assumed to be

$$F = \frac{\sigma_e^2}{\sigma_M^2} - (q_1 f)^2 + 2q_1 f \cosh \frac{3\sigma_m}{2\sigma_M} - \left(1 - \frac{\mu' \sigma_m}{\sigma_M} \right)^2 \tag{16}$$

The results of measurements of Poisson's ratio prior to cavity nucleation in tension and under uniaxial compression (where f = 0) indicate that μ' has a relatively low value when f = 0 which then increases with the cavity volume fraction. This observation has lead to the following proposed expression for μ'

$$\mu' = \mu_1' \frac{(1 - v_C)}{(1 - f)} \tag{17}$$

where μ_1' is the value when cavitation is complete.

6 DETERMINATION OF MODEL PARAMETERS

6.1 GENERAL

In this section, methods are described for determining the parameters in each model from the measurements reported in section 4. Predictions are then made of stress/strain curves under tension, shear and compression and of Poisson's ratio with strain for comparison with experimental results. This will reveal the nature of limitations in the predictive capability of each model.

The results in figures 6 and 7, comparing tensile and shear stress/strain curves for injection moulded specimens and specimens cut from door trim, reveal significant differences in material properties from these two sources. Since the materials models will be used to predict the performance of regions cut from the door trim under impact loading, it was decided, where possible, to use the results from specimens cut from the door trim to determine the properties and parameters required by the models.

6.2 DETERMINATION OF PARAMETERS IN THE VON MISES MODEL

The property requirements for this model have been introduced in section 5.2 and are

- Young's modulus E and elastic Poisson's ratio ν^e
- tensile hardening curves $\sigma_T(\varepsilon_T^p)$ over a range of strain rates.

Figure 9 shows results of measurements on specimens cut from the door trim at a plastic strain rate of 0.01 s^{-1}. Values for E and ν^e were obtained from measurements on specimens having the ISO standard geometry. There is curvature in these results even at very low strains, arising from linear viscoelasticity (see section 6.6). This makes the determination of a Young's modulus ambiguous. The ISO Standard for the determination of tensile properties (1) specifies the gradient of the secant between strains of 0.0005 and 0.0025. This upper strain limit is too low for elastic-plastic analyses which require a strain limit that identifies the onset of significant non-linear behaviour attributable to plastic deformation. We have

selected a strain limit of 0.005 for the polymer studied here, giving a value for E = 1.99 GPa from figure 6. The elastic Poisson's ratio over this strain range is 0.37. The hardening curve at this strain rate was derived from measurements on the specimen (M1S2) which has the waisted geometry shown in figure 2. The elastic component of strain was deducted using equation (5) to give the hardening curve $\sigma_T(\varepsilon_T^p)$ shown in figure 10. The determination of hardening curves at higher strain rates is described in section 6.5.

These results are sufficient to enable the von Mises elastic-plastic model to be used to predict stress/strain curves under uniaxial compressive and shear stresses and the variation of Poisson's ratio with strain. These predictions are compared with experimental data in figures 11 and 12. The door trim is too thin to enable reliable measurements to be made under compression, so the compression data in figure 11 have been obtained on injection moulded specimens as described in section 3.4 and shown in figure 5. Since tensile curves for injection moulded specimens are broadly similar to results obtained on specimens cut from the door trim (figure 6), the compression curve for loading along the axis of the tensile specimen is likely to be representative of compressive behaviour of door trim material. In figure 11, it can be seen that the predicted compressive behaviour coincides with the tensile data and the shear prediction lies below experimental values. In addition, the fall in Poisson's ratio with strain is not predicted by the model, as shown in figure 12. These observations are a direct consequence of the neglect, in the von Mises model, of any influence of the hydrostatic component of the applied stress on yield behaviour. If higher accuracy in predictive capability is required, alternative models should be considered.

6.3 DETERMINATION OF PARAMETERS IN THE LINEAR DRUCKER-PRAGER MODEL

The property requirements for this model have been introduced in section 5.3 and are

- Young's modulus E and elastic Poisson's ratio ν^e
- tensile hardening curves $\sigma_T(\varepsilon_T^p)$ over a range of strain rates
- the hydrostatic stress sensitivity parameter μ
- the flow parameter μ'.

The first two requirements are identical to those for the von Mises model reported in section 6.2. Determination of the parameter μ requires the measurement of hardening behaviour under an additional stress state. Measurements under shear, although not routine, are probably achievable with greater precision than under uniaxial compression. The shear hardening curve for the door trim has been calculated from the shear data in figure 7 and compared with the tensile hardening curve at the same effective plastic strain rate in figure 10.

Through equation (8), yield stresses on each of the curves in figure 10 define a yield surface in 3-dimensional stress space which expands with increasing plastic strain (for a hardening material). Points $\sigma_T,\ \varepsilon_T^p$ on the tensile curve and $\sigma_S,\ \sigma_S^p$ on the shear curve lie on the same surface if the plastic work associated with these points is the same. It can then be shown that

$$\sigma_T\, \varepsilon_T^p \ = \ \sigma_S\, \varepsilon_S^p \tag{18}$$

These points and all others on the yield surface on which they lie are termed equivalent and have the same effective plastic strain. By way of illustration, two pairs of equivalent points are shown on the curves in figure 10 and each pair satisfies equation (18). According to the linear Drucker-Prager criterion equation (8), equivalent stresses σ_S and σ_T are related by the expression

$$\sqrt{3}\ \sigma_S \ = \ \sigma_T\,(\mu+3)/3 \tag{19}$$

which gives

$$\mu \ = \ 3\left[\left(\sqrt{3}\ \sigma_S / \sigma_T\right) - 1\right] \tag{20}$$

The value for μ derived using equation (20) depends upon which pair of equivalent stresses are used and lies in the range 0.8 to 1.0. Using values for μ of 0.5 and 1.0 together with the tensile hardening curve in figure 10 and elastic properties, predictions of shear and compressive stress/strain curves with the linear Drucker-Prager model are compared with experimental data in figures 13 and 14. Whilst the value of μ = 0.5 gives a reasonable

prediction of compressive behaviour a value of $\mu = 1.0$ is needed before shear behaviour is accurately predicted.

A value for the flow parameter μ' can be derived from measurements of the plastic component of Poisson's ratio using equation (11). A typical value for μ' is 0.9 but, as with the determination of μ, the derived value depends on which value of ν_p is chosen for the calculation. This indicates that the Drucker-Prager model cannot reliably predict strain distributions in this polymer which is illustrated by comparisons of measured and predicted curves of Poisson's ratio with tensile strain shown in figure 15.

Figures 13 to 15 illustrate the limitations in the linear Drucker-Prager model for describing the elastic-plastic behaviour of this polymer and the associated uncertainty in the derivation of appropriate values for the model parameters. For an approximate analysis using this model, the set of parameters listed in table 1 are considered likely to give an acceptable description of elastic-plastic behaviour in typical situations.

Table 1 Typical values for the parameters in the linear Drucker-Prager model at a strain rate of 0.01 s^{-1}

E (GPa)	1.99
ν^e	0.37
$\sigma_T(\varepsilon_T^p)$ (MPa)	fig 10
μ	0.8
μ'	0.9

6.4 DETERMINATION OF PARAMETERS FOR THE CAVITATION MODEL

6.4.1 General

The inability of the linear Drucker-Prager model to describe both shear and compressive behaviour and the fall in Poisson's ratio with strain arises because the model does not take account of the nucleation of numerous small cavities on the yield behaviour under a tensile

stress. These cavities nucleate over a range of tensile strain, and this gives rise to the different shape of the tensile curve compared with either the shear or compressive curve as seen in figures 13 and 14 where the tensile hardening curve is used to predict shear and compressive behaviour. The cavitation model attempts to include the influence of cavitation on deformation behaviour through adaption of the yield criterion and the introduction of a cavity nucleation criterion that relates the volume fraction of nucleated cavities to the magnitude of the volumetric strain.

6.4.2 Summary of parameter requirements

The property requirements for this model have been introduced in section 5.4 and are

- Young's modulus E and elastic Poisson's ratio ν^e
- effective shear hardening curves $\sigma_o(\varepsilon_o^p)$ over a range of strain rates. These replace tensile hardening curves in the previous models.
- a hydrostatic stress sensitivity parameter μ
- the volume fraction of cavities v_C in the fully cavitated material
- a cavity interaction parameter q_1
- parameters σ_{MC} and k in equation (13) that describes how the effective shear yield stress σ_o varies with the volume fraction of the phase in which cavities can form
- parameters ε_{1V}, ε_{2V} and β in equation (15) that relates the volume fraction of nucleated cavities f to the volumetric strain produced by the applied stress
- a flow parameter μ'.

6.4.3 Effective yield stresses σ_o

For the cavitation model, hardening behaviour is expressed by a curve of the effective stress σ_o against the effective plastic strain ε_o^p. These quantities are obtained from shear stress (σ_S) and shear strain (ε_S) data in figure 9 using the relationships

$$\sigma_o = \sqrt{3}\,\sigma_S$$

and $$\varepsilon_o^p = \varepsilon_S^p / \sqrt{3} \qquad (21)$$

where ε_S^p is the plastic component of the shear strain and is given, by analogy with equation (5), by

$$\varepsilon_S^p = \varepsilon_S - \frac{\sigma_S}{G} \qquad (22)$$

where G is the shear modulus.

The derived hardening curve for the effective stress at a strain rate of 0.01 s^{-1} is shown in figure 16.

6.4.4 The hydrostatic stress sensitivity parameter μ

Under stress states where no cavities are produced, f = 0 and the yield criterion equation (12) reduces to

$$\frac{\sigma_e}{\sigma_o} = 1 - \frac{\mu\sigma_m}{\sigma_o} \qquad (23)$$

It follows that a value for μ can be derived from measurements of yield stresses under shear and compression using the equation

$$\mu = 3(1 - \sigma_o / \sigma_C) \qquad (24)$$

No attempt was made to carry out compression tests on specimens cut from a door trim moulding because the thickness (2 mm) was insufficient to allow reliable measurements of yield stresses to be made without buckling. Compression tests have however been carried out (section 3.4) on regions cut from injection moulded, tensile specimens. As noted in section 6.2, since tensile stress/strain curves for these specimens are broadly similar to curves for the door trim (see figure 6), then the results of compression tests along the specimen axis

(see figure 5) should be representative of the compressive behaviour of door trim material. The compressive hardening curve (σ_C, ε_C^p) derived from the compression results for the specimen cut along the specimen axis in figure 5, is compared with the effective shear hardening curve (σ_o, ε_o^p) from figure 9 in figure 16. Equivalent stresses σ_o, σ_C are identified to satisfy the plastic work equivalence equation (analogous to equation (18))

$$\sigma_C \, \varepsilon_C^p = \sigma_o \, \varepsilon_o^p \tag{25}$$

A pair of equivalent stresses is shown in figure 16 and, from equation (24), give a value for μ of 0.21.

6.4.5 Volume fraction of cavities v_C when cavity nucleation is complete

The volume fraction of cavities v_C is difficult to estimate because of the variety of sites in the polymer at which cavities could nucleate. A good estimate for v_C can be obtained from accurate Poisson's ratio measurements at strain levels where cavity nucleation is complete and cavity growth is negligible. From these measurements the plastic component ν^p can be calculated using

$$\nu^p = \frac{\nu \varepsilon_T - \nu^e (\varepsilon_T - \varepsilon_T^p)}{\varepsilon_T^p} \tag{26}$$

According to the cavitation model, the plastic component of Poisson's ratio is given by

$$\nu^p = \frac{\left[\dfrac{\sigma_T}{\sigma_{MC}} - q_1 v_C \sinh\left(\dfrac{\sigma_T}{2\sigma_{MC}} \right) - \dfrac{2\mu_1'}{3} \left(1 - \dfrac{\mu_1' \sigma_T}{3\sigma_{MC}} \right) \right]}{\left[\dfrac{2\sigma_T}{\sigma_{MC}} + q_1 v_C \sinh\left(\dfrac{\sigma_T}{2\sigma_{MC}} \right) + \dfrac{2\mu_1'}{3} \left(1 - \dfrac{\mu_1' \sigma_T}{3\sigma_{MC}} \right) \right]} \tag{27}$$

where σ_{MC} and μ_1' are values for σ_M and μ' when cavitation is complete, see equations (14) and (17). The yield criterion (equation (12)) under these conditions with a tensile applied stress gives

$$\frac{\sigma_T^{\,2}}{\sigma_{MC}^{\,2}} - (q_1 v_C)^2 + 2q_1 v_C \cosh\left(\frac{\sigma_T}{2\sigma_{MC}}\right) - \left(1 - \frac{\mu\sigma_T}{3\sigma_{MC}}\right)^2 = 0 \qquad (28)$$

Equation (28) shows that the ratio σ_T/σ_{MC} is determined predominantly by the magnitude of $q_1 v_C$. This means that, from equation (27), the value for Poisson's ratio is determined by the quantities $q_1 v_C$ and μ_1'. Previous studies (5) in which the cavitation model has been applied to the results of tests on a rubber toughened glassy polymer ABS and a propylene-ethylene copolymer, reveal that the parameters q_1 and μ_1' are difficult to determine with any precision and may be broadly independent of the polymer material. We therefore take typical values for $q_1 = 1.5$ and $\mu_1' = 0.17$. It is now possible to use equations (26) and (27) to calculate the variation of Poisson's ratio with tensile strain for different values of v_C for comparison with experimental data. A comparison is shown in figure 17 using a value of $v_C = 0.47$.

6.4.6 Parameters ε_{1V}, ε_{2V}, β and k

These parameters are obtained by an iterative process to achieve satisfactory predictions of the shape of the tensile stress/strain curve in the strain range associated with cavity nucleation. This requires a method for obtaining solutions for the case of uniaxial tension for comparison with experiment. The solutions can be achieved by a finite element analysis applied to a single element with appropriate boundary conditions, but a routine coded on a PC is more convenient. An optimisation procedure for finding the parameter values is not necessary since this is best done by an interactive method for rapidly exploring the effect of changes to the parameters on curve shapes. Figure 18 shows a comparison of measured and calculated tensile curves obtained using the parameters listed in table 2.

Table 2 Values for parameters in the cavitation model at a strain rate of 0.01 s^{-1}

E (GPa)	1.99
ν^e	0.37
$\sigma_o\left(\varepsilon_o^p\right)$ (MPa)	fig 16
μ	0.21
v_C	0.47
k	2.55
σ_{MC} (MPa)	94 (from eqn (13))
q_1	1.5
μ_1'	0.17
ε_{1v}	0.0022
ε_{2v}	0.01
β	0.5

6.5 RATE DEPENDENT PLASTICITY

6.5.1 General

Whichever model is used for a stress analysis, more accurate predictions will be made if the dependence of properties on strain rate is taken into consideration. In many finite element systems, facilities are available for including the dependence of yield behaviour on strain rate (rate-dependent plasticity). There are problems with the measurement of properties at impact strain rates (> 100 s^{-1}) arising from the effects of resonances in the specimen and test assembly. A method is described in this section for the determination of properties at high strain rates by modelling behaviour at low and moderate rates and calculating high rate behaviour by extrapolation. The method is illustrated in subsection 6.5.2 using the results of tests on injection moulded specimens. Properties for the door trim material are derived from additional tests in 6.5.3.

The rate dependence of low-strain (linear viscoelastic) behaviour is in general not included in elastic-plastic models, but brief reference is made in section 6.6 showing how the rate-dependence of a stress/strain curve can be related to stress relaxation results.

6.5.2 Injection moulded material

6.5.2.1 Tensile behaviour

The characterisation of plastic behaviour for elastic-plastic models requires determination of a hardening function $\sigma(\varepsilon^p)$, which is most conveniently measured in tension (see section 5.1). In finite element analyses where the dependence of plastic deformation on strain rate needs to be included, it is necessary to determine the variation in the hardening curve with strain rate. A procedure is now described for determining properties by

- modelling the shape of experimental hardening curves at low and moderate strain rates
- determining the variation of model parameters with strain rate
- and deriving hardening behaviour at high strain rates by extrapolation.

Stress/strain curves measured in tension over a range of strain rate are shown in figure 19. These were obtained on waisted specimens of the geometry shown in figure 2 cut from the central region of injection moulded standard tensile specimens. Hardening curves $\sigma_T(\varepsilon_T^p)$ derived from these data (see section 5.1) are shown in figure 20. These curves have been fitted using the function

$$\sigma_T(\varepsilon_T^p) = \sigma_i + (\sigma_f - \sigma_i)\left(1 - \exp - (\varepsilon_T^p / \varepsilon_a)^\beta\right) \qquad (29)$$

where σ_i is the stress at zero plastic strain, σ_f is the limiting stress at high plastic strains and ε_a and β are parameters that determine the mean strain and the strain range over which the increase of σ_T with ε_T^p occurs. Values for the parameters used to obtain the fits in figure 20 are shown in table 3.

Table 3 Values for the parameters in equation (29) used to obtain the fits to tensile data in figure 20

Plastic strain rate (s^{-1})	σ_f (MPa)	σ_i	ε_a	β
12	28.6	11.5	0.007	0.8
1.5	26.1	10.5	0.007	0.8
0.15	23.6	9.5	0.007	0.8
0.013	21.3	8.5	0.007	0.8
0.001	18.8	7.5	0.007	0.8

The calculated curves were obtained with a constant value for ε_a and β and an approximately constant ratio of $\sigma_i/\sigma_f = 0.4$. Although these fits are adequate, it is evident that the peak stress is reached at lower plastic strains as the strain rate increases, implying that ε_a is decreasing with strain rate. Better fits can, accordingly, be obtained with the parameters given in table 4 as shown in figure 21.

Table 4 Repeat of table 3 but with values for ε_a decreasing with strain rate to give better fits to experimental data

Plastic strain rate (s^{-1})	σ_f (MPa)	$\sigma_i = 0.4\ \sigma_f$	ε_a	β
12	28.6	11.5	0.006	0.8
1.5	26.1	10.5	0.007	0.8
0.15	23.6	9.5	0.008	0.8
0.013	21.3	8.5	0.009	0.8
0.001	18.8	7.5	0.01	0.8

The increase in σ_f with plastic strain rate can be described by the Eyring function.

$$\sigma_f = \sigma_{fo} + A \log \dot{\varepsilon}_T^p \qquad (30)$$

where σ_{fo} and A are material parameters. This is demonstrated in figure 22 which gives values for σ_{fo} = 25.7 MPa and A = 2.3 MPa when strain rate is in units of s^{-1}. The variation of ε_a can be described by a similar function

$$\varepsilon_a = \varepsilon_{ao} - B \log \dot{\varepsilon}_T^p \qquad (31)$$

with ε_{ao} = 0.007 and B = 0.001.

Equations (29), (30) and (31) together with a knowledge of 6 material parameters (σ_{fo}, A, σ_i/σ_f, ε_{ao}, B and β) can therefore be used to derive tensile hardening curves at any arbitrary strain rate. This information constitutes the hardening properties required by an analysis with rate dependent plasticity using the von Mises or linear Drucker-Prager models. (Note, the cavitation model requires hardening properties in the form of effective shear data). If a lower accuracy in describing the shape of hardening curves at strains below 0.04 is acceptable, then the number of parameters reduces to 5 (σ_{fo}, A, σ_i/σ_f, ε_a and β). Curves at high strain rates associated with impact speeds calculated using the parameters listed in table 4 are shown in figure 21. The precision of these data depends upon the validity of the extrapolation using equation (30) beyond the range of measured values in figure 22 and is a subject for further study.

6.5.2.2 Shear behaviour

Plastic strain hardening in the cavitation model is defined by hardening curves determined under a shear stress (see sections 5.4 and 6.4.3). Stress/strain curves measured at different strain rates are shown in figure 23. Hardening behaviour is expressed by a curve of the effective stress σ_o against the effective plastic strain ε_o^p (see section 6.4.3). Hardening curves for the effective stress have been derived from the data in figure 23 and are shown in figure 24.

Using the same function equation (29) that was used to model tensile behaviour, the curves in figure 24 have been modelled using the equation

$$\sigma_o(\varepsilon_o^p) = \sigma_{oi} + (\sigma_{of} - \sigma_{oi})\left(1 - \exp - (\varepsilon_o^p / \varepsilon_{oa})^{\beta_o}\right) \qquad (32)$$

Values for the parameters in equation (32) are shown in table 5.

Table 5 Values for the parameters in equation (32) used to fit the shear data in figure 24

Strain rate (s^{-1})	σ_{of} (MPa)	σ_{oi} (MPa)	ε_{oa}	β_o
0.1	29.5	11.5	0.009	0.75
0.017	27.3	10	0.009	0.75
0.0017	23.1	9.5	0.009	0.75
0.00017	19.5	7.5	0.009	0.75

Constant values for the parameter ε_{oa} in table 3 show that, in contrast to tensile results, the hardening curve shape remains constant with strain rate and simply shifts up the stress axis with increasing rate. It can be seen from the results in table 5 that the ratio σ_{oi}/σ_{of} may be assumed constant at a value of 0.4. Values for σ_{of} from table 5 are plotted against log plastic strain rate in figure 25 and are compared with tensile data from figure 22. The variation of σ_{of} with log strain rate $\dot{\varepsilon}_o^p$ is again accurately linear and can be represented by the equation, analogous to equation (30),

$$\sigma_{of} = \sigma_{ofo} + C \log \dot{\varepsilon}_o^p \qquad (33)$$

where, from figure 25, σ_{ofo} = 33.1 MPa and C = 3.6.

The results in figure 25 show that the ratio of tensile and effective shear stresses when cavitation is complete varies with strain rate. The probable reason for this is that the cavity

volume fraction when cavity nucleation is complete increases with strain rate. This conclusion is supported by measurements of Poisson's ratio at very low test speeds. These results show a smaller drop in value than is observed in results at higher speeds (figure 17) which is consistent with a lower value for v_C. As the strain rate is lowered, the shear yield stress decreases thereby promoting shear yielding in favour of cavitation in certain regions of the polymer. At higher rates, cavitation takes place in these regions but there will presumably be a limit to the increase in v_C with strain rate when cavities have formed in all the available regions in the polymer. This means that, at higher strain rates, the gradient of the tensile line should increase thereby introducing some uncertainty in the linear extrapolation of equation (30).

This issue is considered further in the next subsection that deals with the determination of rate-dependent plastic behaviour for the door trim material.

6.5.3 Door trim material

6.5.3.1 Shear behaviour

Figure 26 shows values for effective shear flow stresses and tensile flow stresses obtained at different strain rates on specimens cut from a door trim. The panel was different from those used to obtain the results shown earlier in this report in figures 6 and 7. The Eyring fit to the effective shear data in figure 26 has a higher slope compared with the effective shear results for the injection moulded material in figure 25. This is consistent with a higher flow stress for the door trim material, as observed in figure 7. The intercept on the log strain rate axis is the same for both materials indicating that the mechanisms giving rise to the increase in the yield stresses for the door trim material are independent of strain rate.

Use of the Eyring equation (33) to describe the dependence of flow stress σ_{of} on strain rate for the door trim gives values for σ_{ofo} and C listed in table 6. These values are needed to model rate-dependent plasticity for use with the cavitation model in a finite element analysis. Also needed are parameters σ_{oi}, ε_{oa} and β_o in equation (32) used to describe the hardening behaviour of the effective yield stress σ_o (see figure 16). Values for these parameters for the

door trim are also shown in table 6 obtained by fitting equation (32) to the shear data in figure 16.

Table 6 Values for the parameters in equations (32) and (33) used to model rate-dependent plasticity in shear for the door trim material

σ_{ofo} (MPa)	36.8
C (MPa)	4.0
σ_{oi} (MPa)	0.4 σ_{of}
ε_{oa}	0.007
β_o	0.7

6.5.3.2 Tensile behaviour

Results of measurements of tensile flow stress of the door trim material at different strain rates are also shown in figure 26. Although there is relatively higher scatter in these values compared with the injection moulded specimen results in figure 25, there is an indication that the Eyring fit has a different intersection on the log strain rate axis than the fit to the effective shear data implying, as with the injection moulded material, a dependence of the volume fraction, v_C, of cavities when nucleation is complete on strain rate. As explained in section 6.5.2.2, the value for v_C must reach a constant value at high strain rate. The rate-dependence of the tensile flow stress for the door trim material has therefore been described in figure 26 by an Eyring fit that passes through the intercept of the effective shear results on the log strain rate axis. This line represents behaviour for which v_C is independent of strain rate and is consistent with a value for v_C at high rates. The fit represents the Eyring function, equation (30), for tensile behaviour of the door trim polymer and gives values for the parameters σ_{fo} and A shown in table 7. These values are needed to model rate-dependent plasticity for use with the von Mises and linear Drucker-Prager models in a finite element analysis. Also needed are parameters in equation (29) used to describe the hardening behaviour under tension. These parameters are σ_i, ε_a and β and have been derived from the tensile data in figure 10. They are given for the door trim material in table 7 and are assumed to be independent of strain rate to a reasonable approximation.

Table 7 Values for the parameters in equations (29) and (30) used to model rate-dependent plasticity in tension for the door trim material

σ_{fo} (MPa)	24.7
A (MPa)	2.7
σ_i (MPa)	0.4 σ_f
ε_a	0.0045
β	0.8

Using equations (32) and (33) with the parameters given in table 6 to characterise the rate-dependent effective shear hardening behaviour of the door trim material, a hardening curve can be calculated for a strain rate of 10 s^{-1}. This was used with the cavitation model to calculate a tensile stress/strain curve which is compared with an experimental curve in figure 27. The values for the cavitation model parameters used in this calculation are listed in table 8. The only parameters that have changed from the values listed in table 2 for a strain rate of 0.01 s^{-1} are E, v_C and ε_{2V}. The value for E appropriate to the higher rate of 10 s^{-1} was estimated from results for the variation of tensile behaviour of injection moulded material with strain rate shown in figure 19. Values for v_C and ε_{2V} in table 8 were chosen to give the best fit to the experimental tensile date at 10 s^{-1}. The slightly higher value for v_C (0.48 over 0.47) supports the conclusions drawn in section 6.5.2.2 that v_C is increasing with strain rate and implies that this increase has slowed and may have stopped at rates of 10 s^{-1} and above. The decrease in ε_{2V} at the higher rate implies that the nucleation of cavities takes place over a smaller range of volumetric strain at the higher rate and may be consistent with the observed change in the shape of the tensile hardening curve with strain rate (decrease in ε_a) for the injection moulded material seen in figure 20.

Table 8 Values for parameters in the cavitation model used to calculate tensile behaviour at a strain rate of 10 s^{-1} (see figure 27)

E (GPa)	2.45
ν^e	0.37
σ_{of} (MPa)	40.8
σ_{oi} (MPa)	16.3
ε_{oa}	0.007
β_o	0.7
μ	0.21
ν_C	0.48
k	2.55
q_1	1.5
μ_1'	0.17
ε_{1V}	0.0022
ε_{2V}	0.005
β	0.5

6.6 RATE-DEPENDENT ELASTICITY

Stress/strain curves in constant strain rate tests on viscoelastic materials are not straight lines even at low strains where behaviour is linear. This arises because properties depend upon time under load which is changing throughout the test. The ISO standard for tensile testing specifies the determination of a tensile (secant) modulus which is the gradient of the line joining points on the curve at strains of 0.0005 and 0.0025. This gradient changes with the strain rate and hence speed of the test. This is not a rigorous characterisation of low-strain behaviour but is satisfactory for glassy polymers that are only slightly viscoelastic. Where greater precision is required, the shape of a stress/strain curve over the range of strains where behaviour is linear viscoelastic can be related to results from a single stress relaxation test.

A stress relaxation function under tension E(t) relates the time varying stress $\sigma(t)$ to the tensile strain ε under a situation where the strain is held constant with time. So

$$\sigma(t) = E(t)\varepsilon \tag{34}$$

A tensile test consisting of monotonic loading under a constant strain rate can be considered as a series of step increases in strain with strain increment $\Delta\varepsilon$ for periods Δt. For strain levels where behaviour is linear, the stress response to the step loading can be derived by superposition as follows

$$\sigma(t) = E(t)\,\Delta\varepsilon + E(t-\Delta t)\,\Delta\varepsilon + E(t-2\Delta t)\,\Delta\varepsilon + \ldots \tag{35}$$

The situation where the strain is applied smoothly at constant velocity can be realised by letting $\Delta\varepsilon \rightarrow 0$ in which case equation (35) reduces to the integral equation

$$\sigma(t) = \int_o^t E(t-s)\,\frac{d\varepsilon}{ds}\,ds \tag{36}$$

where s is a dummy time variable.

By defining a new time variable u = (t - s) and noting that $d\varepsilon/ds = \dot{\varepsilon}$, equation (36) becomes

$$\sigma(t) = \dot{\varepsilon}\int_o^t E(u)\,du \tag{37}$$

Stress relaxation data for the Dow polymer are shown in figure 28 and have been quite accurately modelled by the function

$$E(u) = E_R + D\,u^{-n} \tag{38}$$

where E_R = 820 MPa, D = 740 MPa.s^n and n = 0.17.

Inserting equation (38) into (37) and noting that $\dot{\varepsilon} = \varepsilon / t$ gives the equation of a stress/strain curve under constant strain rate as

$$\sigma(\varepsilon) = E_R \varepsilon + \frac{D\dot{\varepsilon}^n \varepsilon^{1-n}}{1-n} \qquad (39)$$

Equation (39) captures the non-linear variation of stress with strain and the dependence on strain rate. Predicted curves at selected strain rates are shown in figure 29 and compared with experimental data at a strain rate of 0.01 s^{-1}. The departure of predicted and measured values at strains above 0.005 implies that this strain level marks the limit of linear viscoelastic behaviour. It should be noted that values for the parameters in the stress relaxation function, equation (38), were obtained by comparison with experiment at times > 1s. The applicability of these values at times << 1s is not known so the accuracy of predicted stress/strain behaviour in figure 29 at high strain rates is uncertain.

7 CONCLUDING SUMMARY

Finite element systems use elastic-plastic models to describe the non-linear, large-strain behaviour of rigid materials. Although not developed for plastics materials, these models can be used to predict forces and deformations associated with a component under impact loading. The accuracy of predictions will depend on the suitability of the model for the polymer being studied and the accuracy achieved in the determination of model parameters.

The elastic-plastic model based on the von Mises yield criterion is the simplest model but neglects any influence of the hydrostatic component of stress on yield behaviour. The data requirements for this model can be derived from tensile tests alone and are a Young's modulus, a Poisson's ratio and tensile hardening curves. Since the yield behaviour of plastics depends on strain rate, for maximum accuracy in predictions, these curves should be determined over a range of strain rates relevant to the application. Tensile hardening curves for injection moulded material are shown in figure 20 and can be modelled using equations (29) and (30).

Values for Young's modulus and Poisson's ratio for the door trim material are given in table 1 at a strain rate of 0.01 s^{-1}. The Young's modulus will increase with strain rate, and a higher value should ideally be used for impact simulations which can be derived from the data in figure 19. The variation of tensile hardening curves with strain rate for the door trim

material can be calculated using equations (29) and (30) with the parameter values given in table 7.

The linear Drucker-Prager model is more accurate for plastics than the von Mises model since it accounts for some influence of the hydrostatic component of stress on yield behaviour. Determination of the parameters for this model requires data from tests in tension and one other stress state such as shear or compression. Whilst this model accounts for different yield stresses in tension and compression, it is not possible to accurately predict stress/strain behaviour, under shear and compression, and Poisson's ratio for materials that exhibit significant cavitation (void formation) under tensile stress states.

Values for the parameters for the door trim material in the linear Drucker-Prager model are given in table 1 at a low strain rate. The shape of the hardening curve and its variation with strain rate can be modelled using equations (29) and (30), respectively. Values for the parameters in these equations for the door trim are given in table 7. Young's modulus at higher strain rates can be estimated from the data in figure 19. Since values for the other parameters cannot be obtained with high precision, it is not possible to evaluate their dependence on strain rate.

The cavitation model takes account of the nucleation of cavities on yield behaviour under stress states where there is a significant hydrostatic component. Cavities nucleate in the more mobile regions of the polymer, which in the materials studied here are presumably the amorphous phase and the rubber toughening particles. Debonding at the interface with filler particles may also contribute to the overall effective volume fraction of voids. The nucleation of cavities is assumed to be determined by the level of volumetric strain and to take place over a range of volumetric strain for a distribution in the size of the mobile regions.

Values for the parameters for the door trim material in the cavitation model are given in table 2 at a low strain rate. The hardening behaviour in this model is characterised by the effective shear stress against effective shear plastic strain curve. The variation in hardening behaviour with strain rate is given by equations (32) and (33) with the parameter values listed in table 6. The value of Young's modulus E will also increase with strain rate, and values at higher rates can be estimated from the results in figure 19. In this context, it should be noted

that the gauge length of the extensometer used for the acquisition of these data was 4 mm. If accurate modulus measurements are required, additional tests using the ISO specimen with a larger gauge length should be employed. The variation of modulus with strain rate can be investigated using a linear viscoelastic analysis (see section 6.6) with experimental stress relaxation data. This analysis demonstrates that the concept of a Young's modulus is ambiguous for a viscoelastic material. Using this analysis, it is only possible to calculate the modulus values at high rates using equation (39) if the stress relaxation parameters in this equation were obtained from experiment at very short times.

The parameters v_C and ε_{2V} appear to vary slowly with strain rate, and, for impact simulations, it may be more appropriate to employ the parameter values list in table 8 despite these being based on tensile results at a strain rate of 10 s^{-1} which have lower accuracy than measurements obtained at a lower test speed.

Shear and tensile moduli determined on specimens cut from door trim mouldings are higher than values obtained on injection moulded specimens. Although these sources of test specimens are supposed to be from the same grade of polymer, it is difficult to explain how these increases can be attributed to different moulding conditions. The shear flow stress for the door trim material is also higher than the flow stress for injection moulded material. The tensile flow stress is similar for both materials but peaks at a lower strain for the door trim. These observations require a larger value for the volume fraction of cavities v_C when cavitation is complete in the door trim and revised cavity nucleation parameters that indicate that cavities form at lower strains in the door trim.

8 ACKNOWLEGEMENT

This work was funded by the Department of Trade and Industry as part of the Measurement for Processing and Performance programme. The authors would like to acknowledge the assistance of Elena Arranz with some of the measurements in shear and tension.

9 REFERENCES

1. ISO 527-2, Plastics – Determination of tensile properties – Part 2: Test conditions for moulding and extrusion plastics.

2. G Dean and L Wright. Analysis of failure tests on uniaxial tensile and plate specimens of ABS. NPL report MATC(A)88, April 2002.

3. M Arcan, Z Hashin and A Veloshin. Exp. Mech., (1978) vol.18, p 141.

4. B Read and G Dean. Modelling non-linear stress-strain behaviour of rubber toughened plastics. Plastics, Rubber and Composites (2001) vol.30, p 328.

5. G Dean, B Read and L Wright. A comparison of the data requirements and predictive accuracy of the cavitation model and a simple model for non-linear behaviour. NPL report MATC(A)120, September 2002.

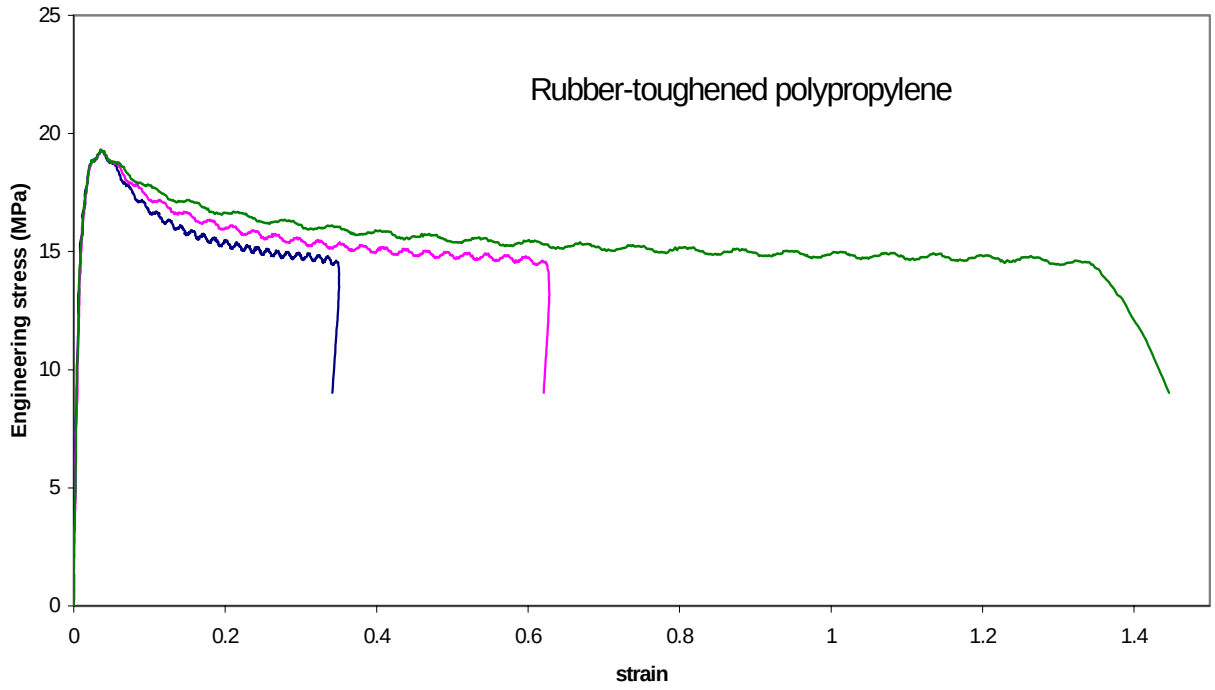

Figure 1 Engineering stress/strain curves measured in a tensile test on a standard tensile specimen. A gauge length of 10 mm was used at 3 separate locations along the length of the specimen.

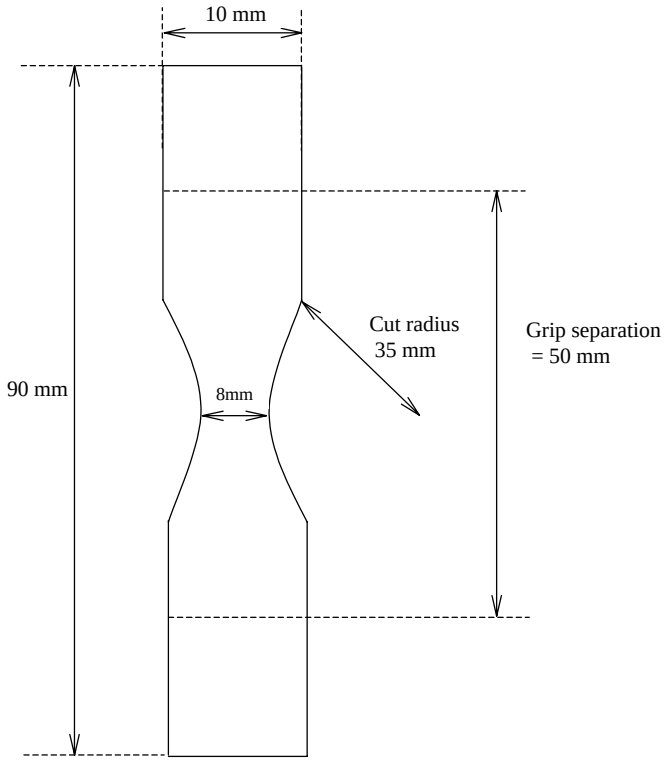

Figure 2 Specimen geometry for the measurement of tensile behaviour at large strains.

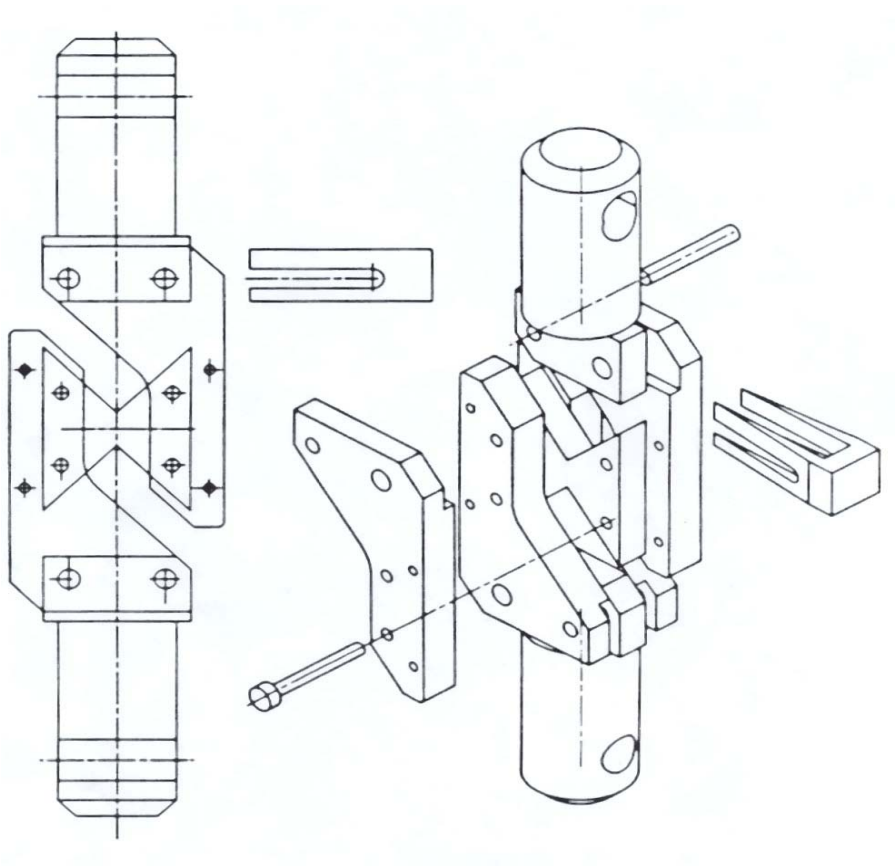

Figure 3 Test assembly for the measurement of shear stress/strain curves using the notched plate method.

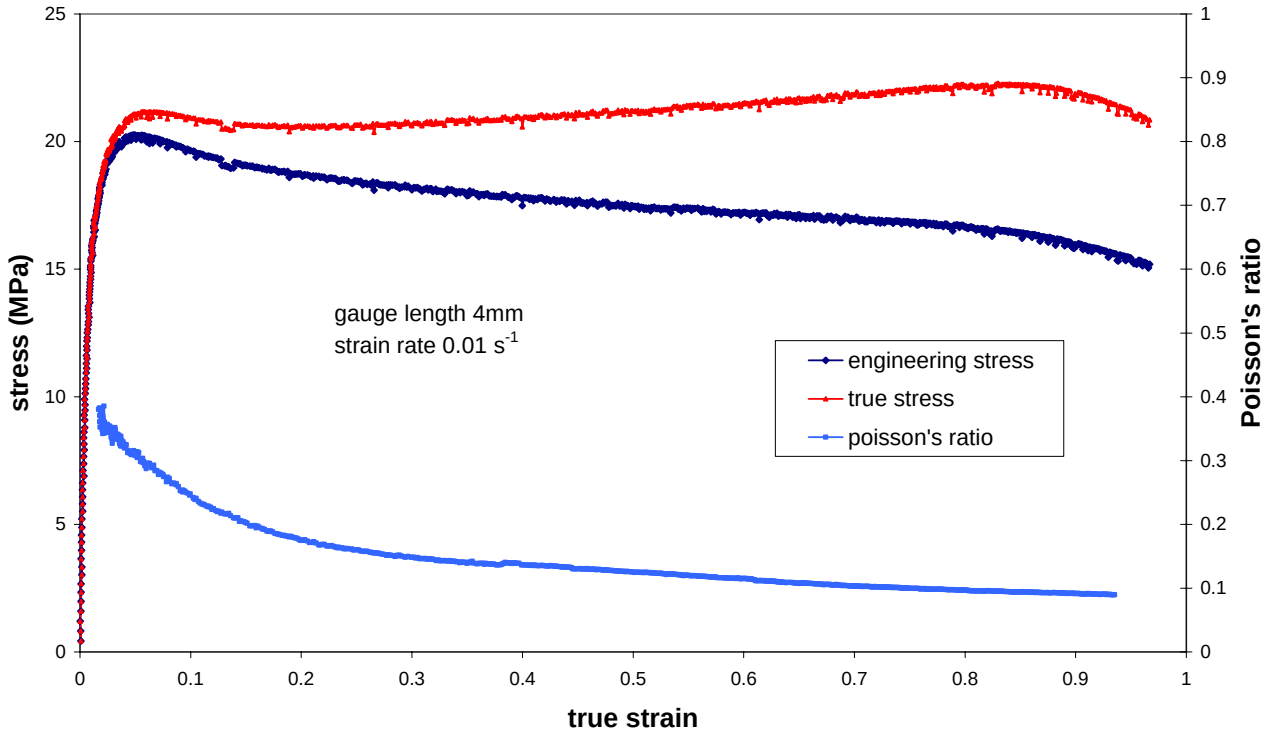

Figure 4 Tensile results obtained using the new specimen geometry cut from the central region of a standard injection moulded tensile specimen.

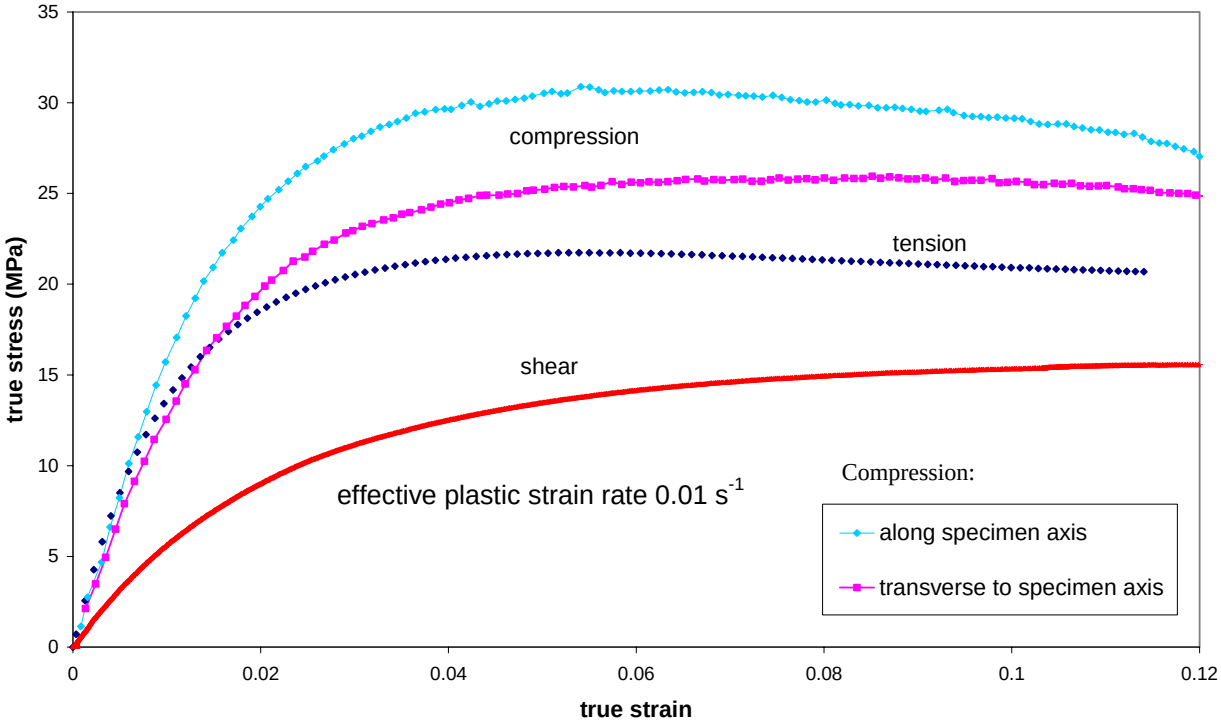

Figure 5 Comparison of tensile, shear and compressive stress/strain curves obtained on injection moulded specimens at a plastic strain rate of 0.01 s^{-1}.

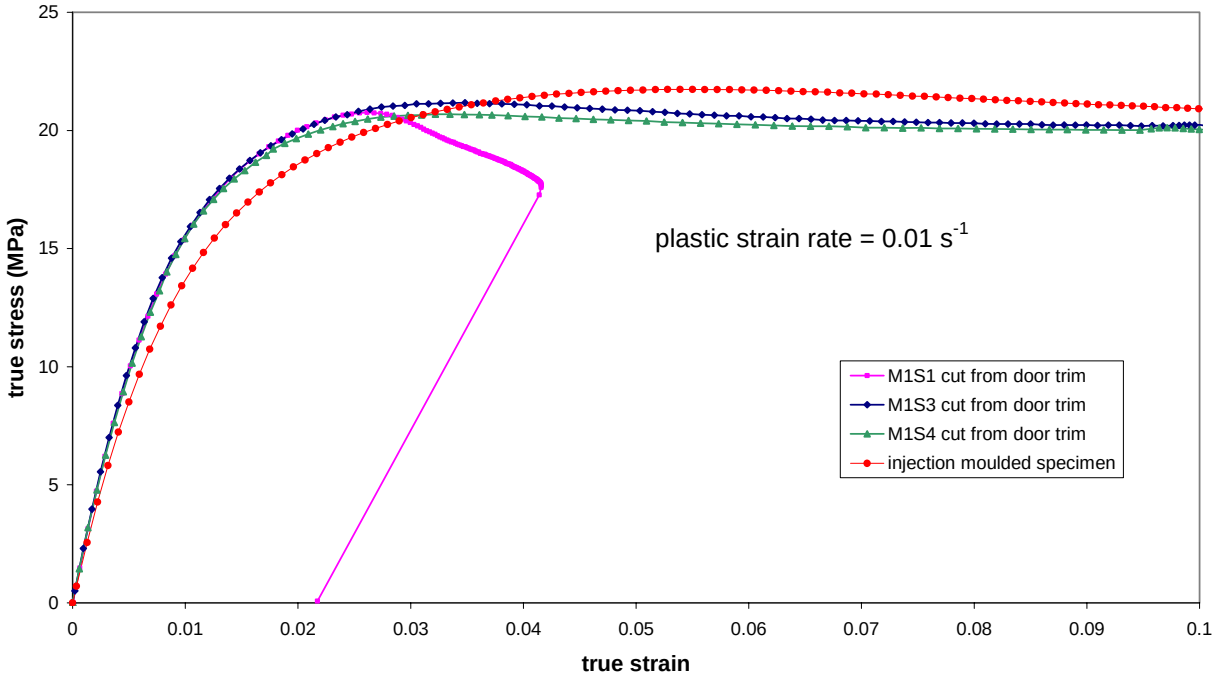

Figure 6 Comparison of tensile measurements obtained on an injection moulded specimen with results from specimens cut from door trim – ISO specimen geometry.

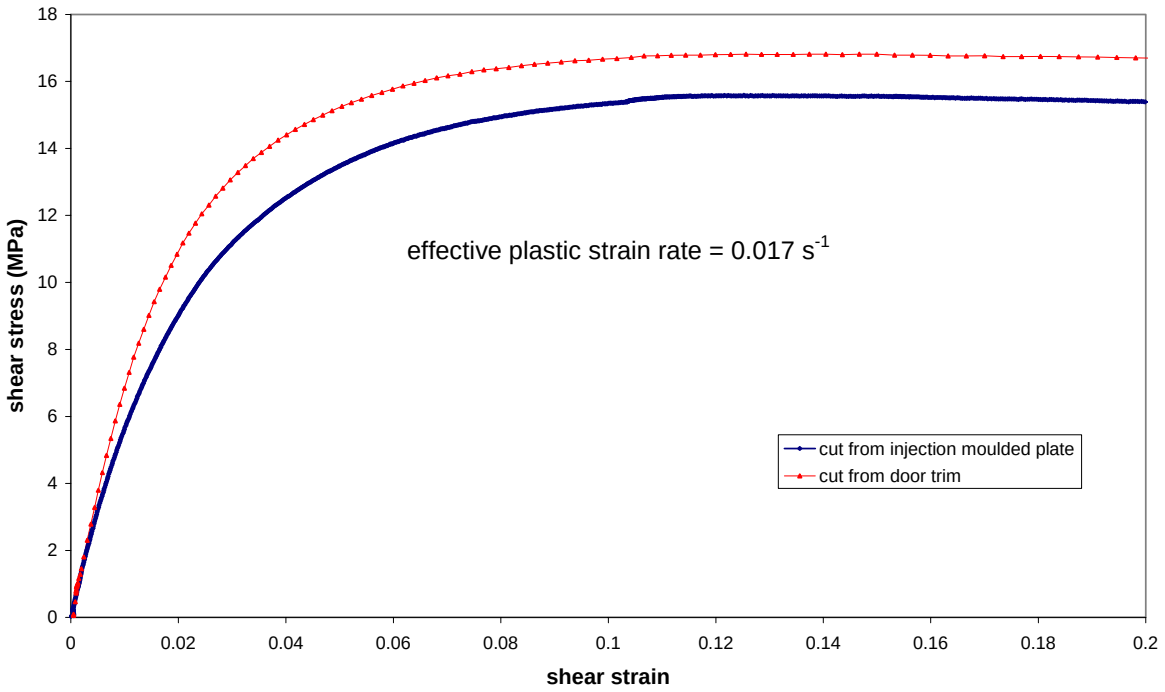

Figure 7 Comparison of shear measurements obtained on an injection moulded plate with results from specimens cut from door trim.

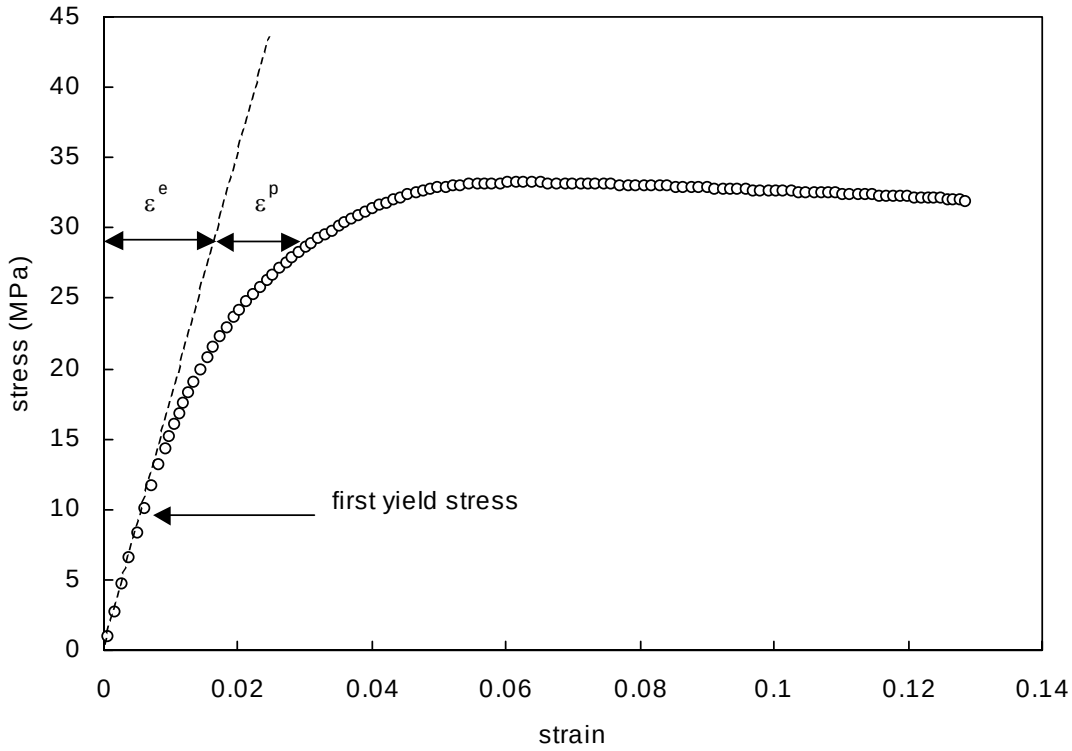

Figure 8 Schematic diagram showing how the total strain in elastic-plastic models is the sum of elastic and plastic components.

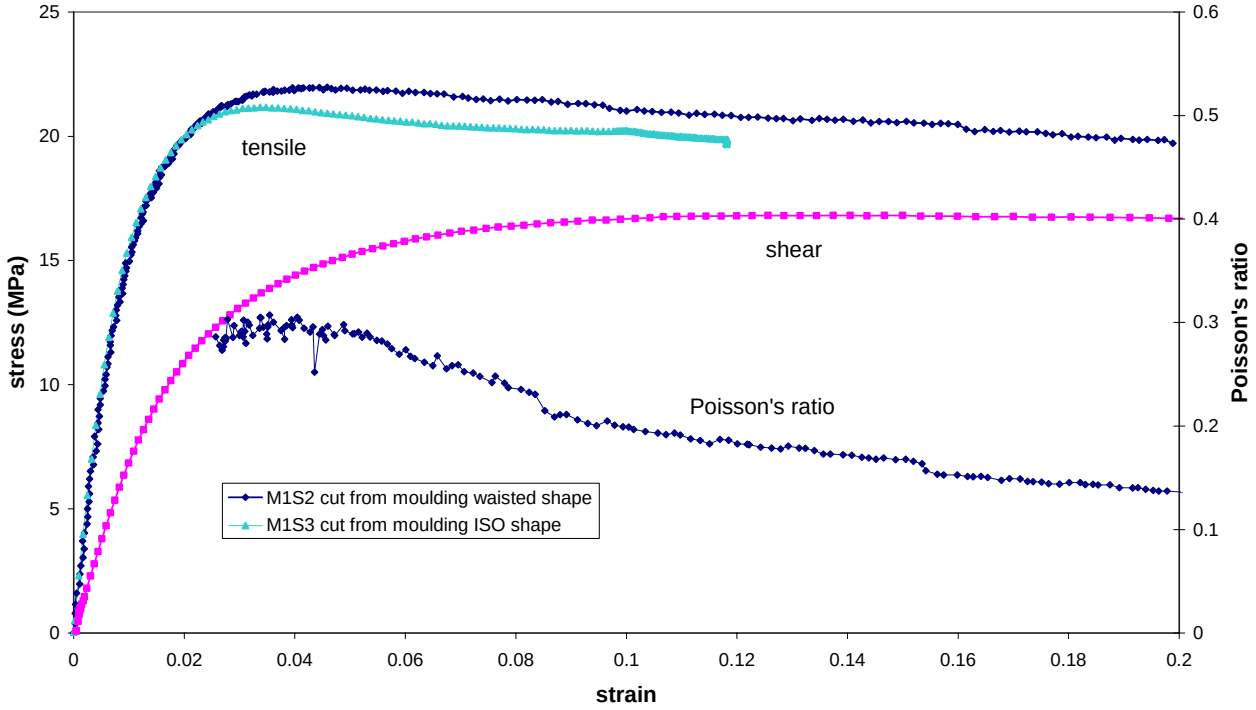

Figure 9 Results of tensile and shear measurements at a strain rate of 0.01 s^{-1} on specimens cut from a door trim moulding.

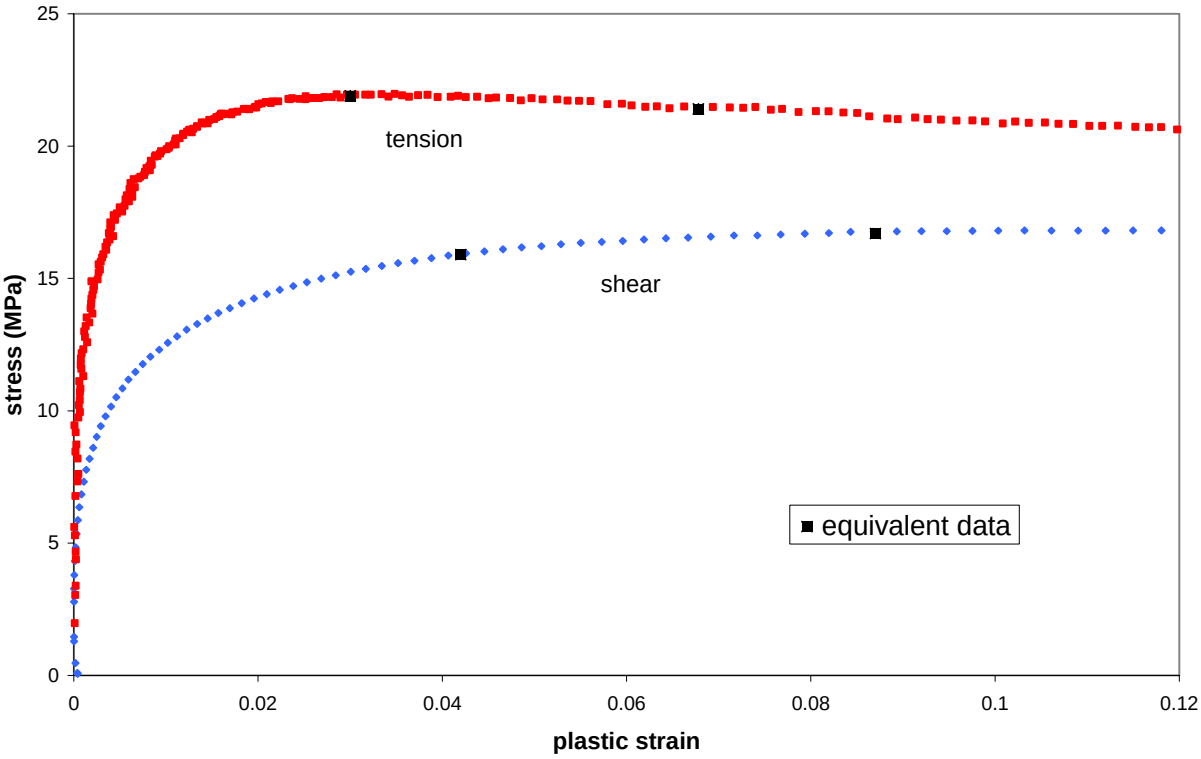

Figure 10 Hardening curves derived from the tensile and shear results in figure 9.

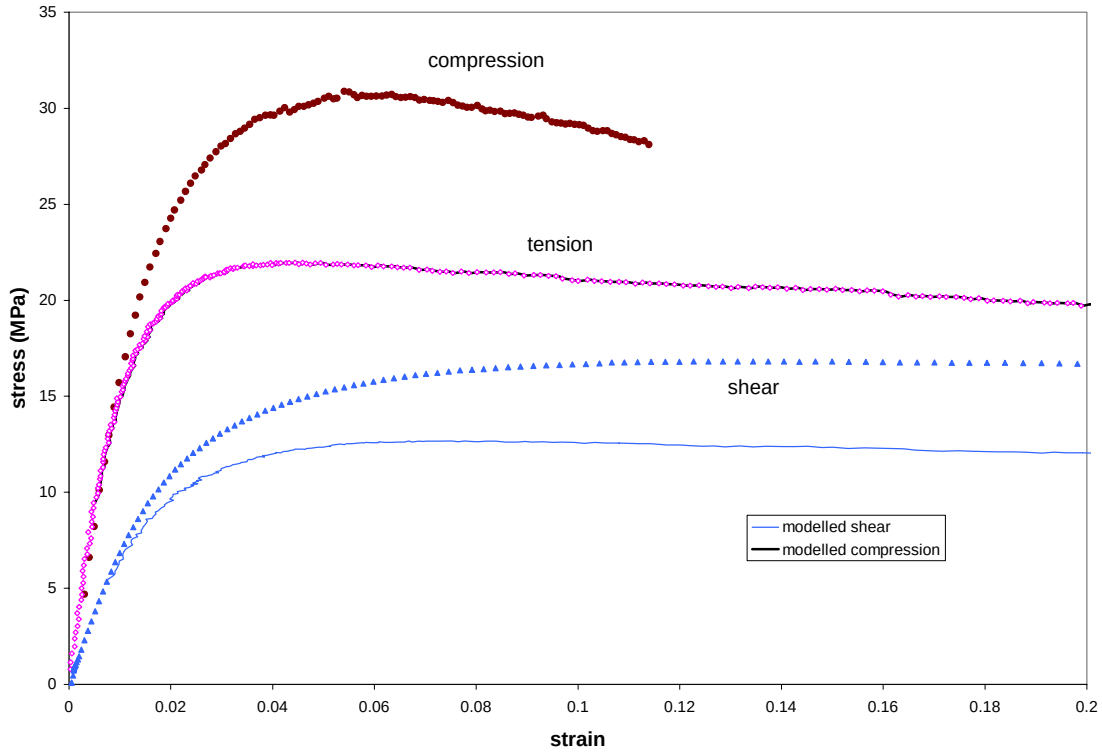

Figure 11 Comparison of compressive and shear stress/strain curves predicted using the von Mises model with experimental data.

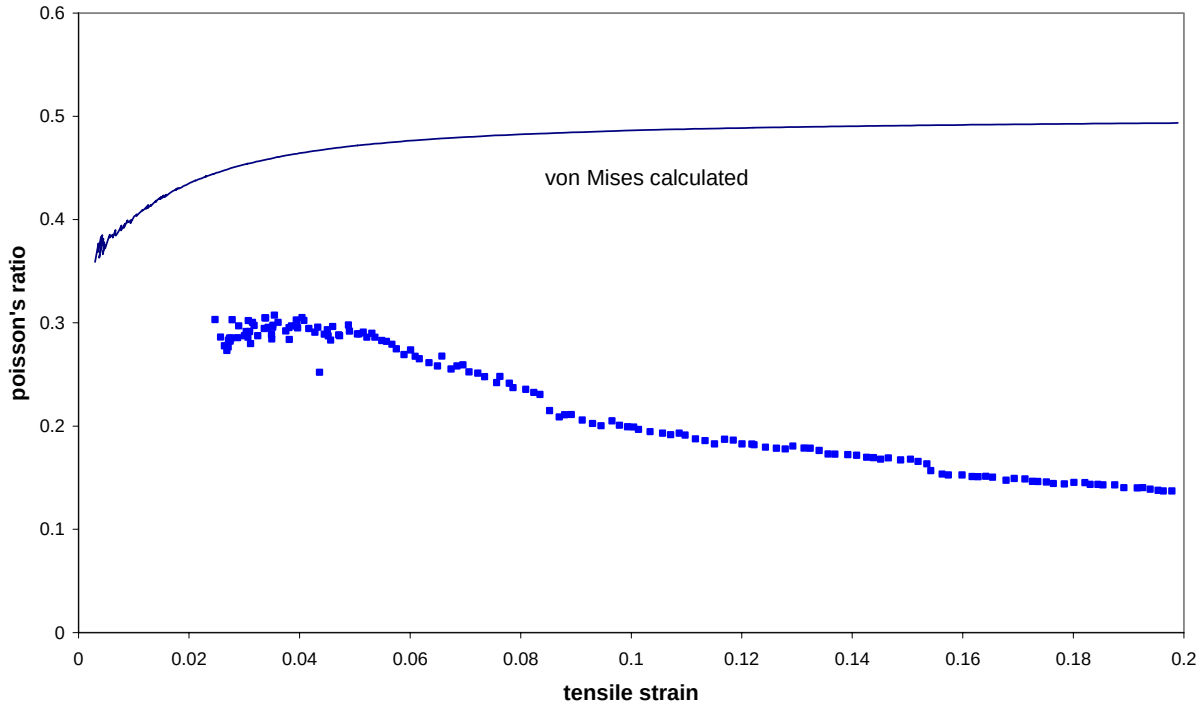

Figure 12 Comparison of Poisson's ratio values predicted using the von Mises model with experiment.

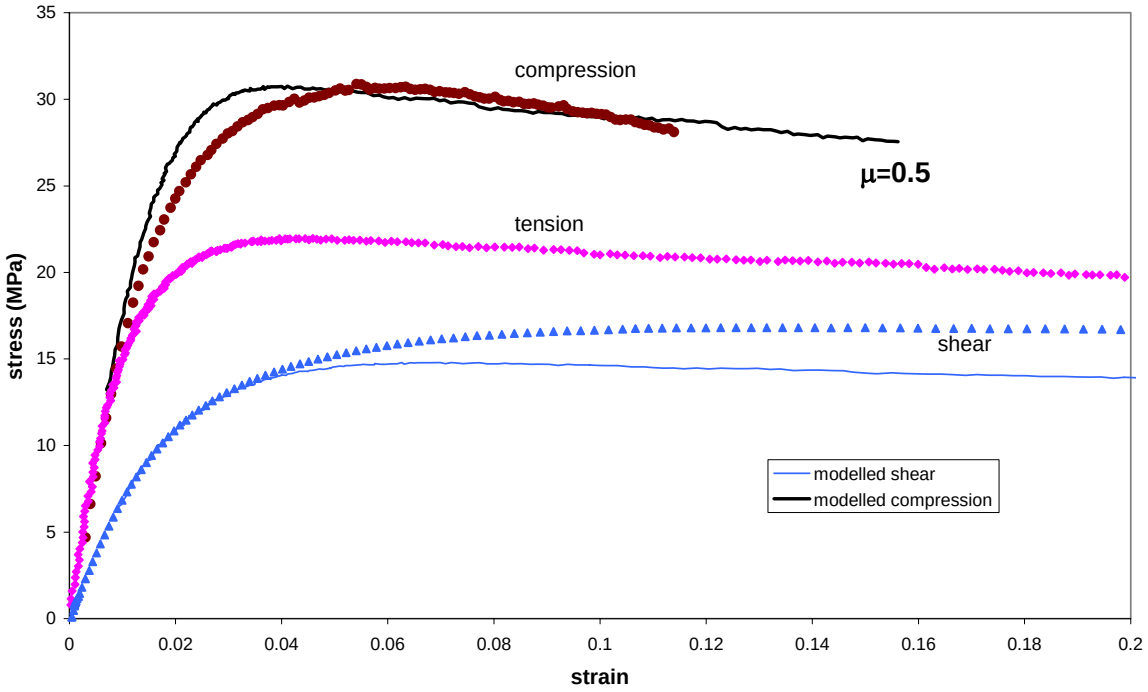

Figure 13 Comparison of measured compressive and shear stress/strain results with curves predicted using the linear Drucker-Prager model with μ = 0.5.

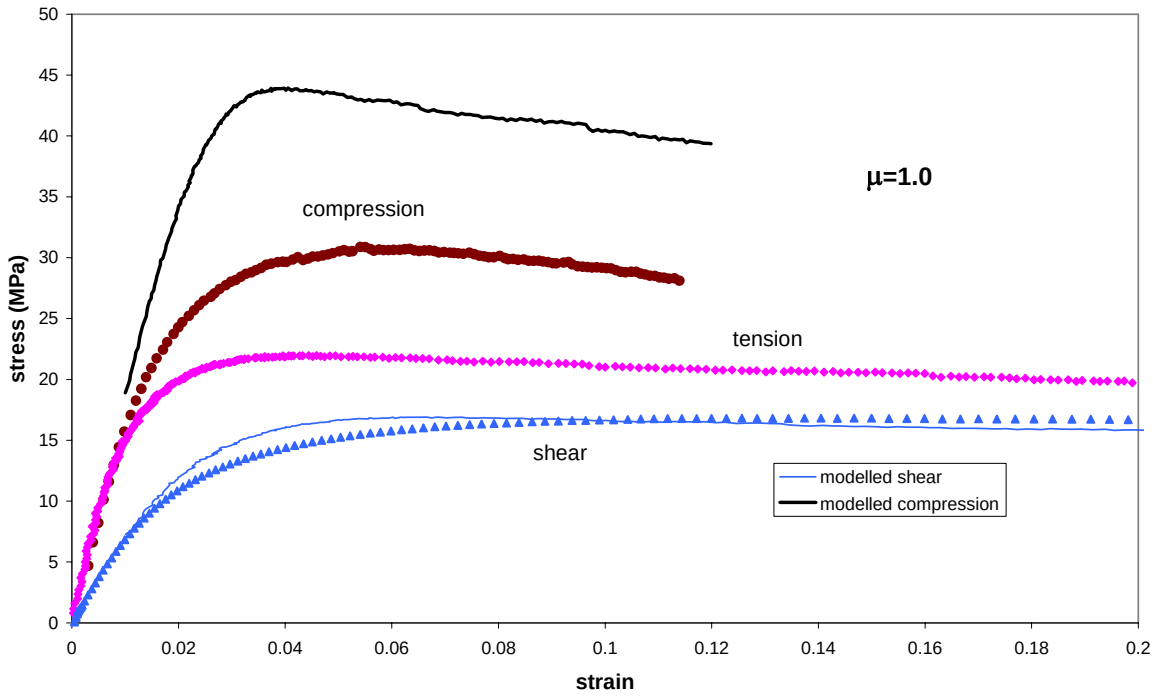

Figure 14 Comparison of measured compressive and shear stress/strain results with curves predicted using the linear Drucker-Prager model with μ = 1.0.

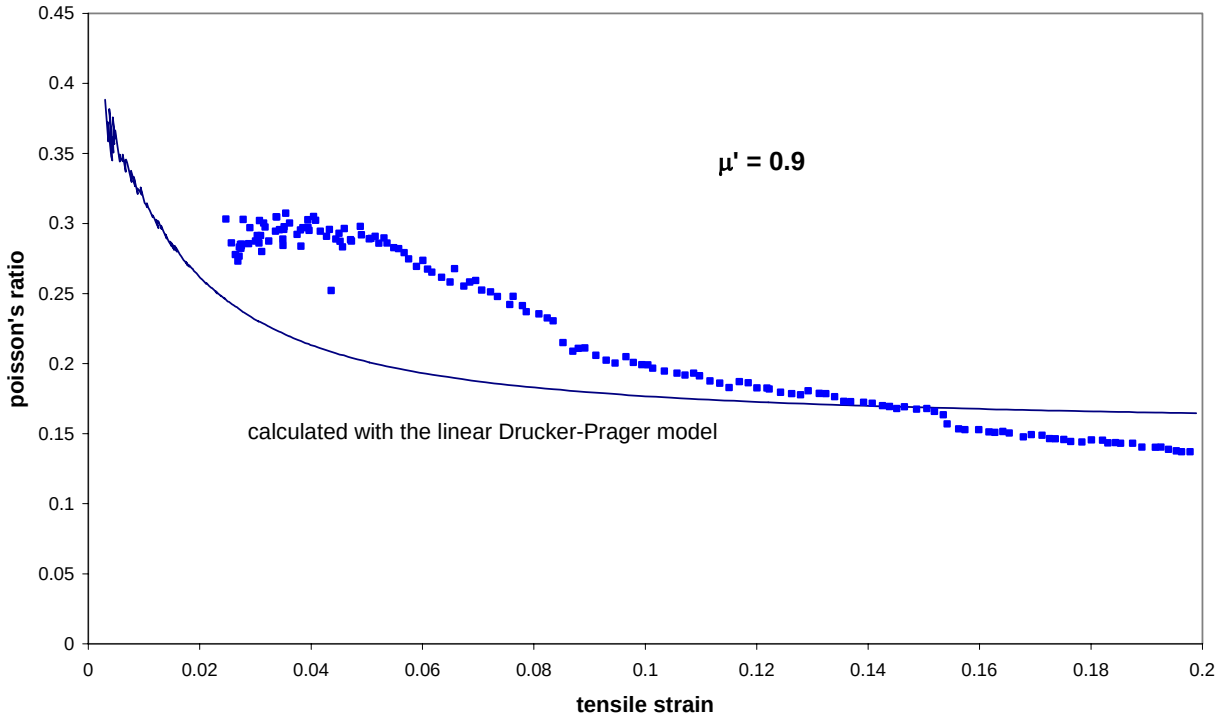

Figure 15 Comparison of Poisson's ratio measurements with results predicted using the Linear Drucker-Prager model using a value for μ' = 0.9.

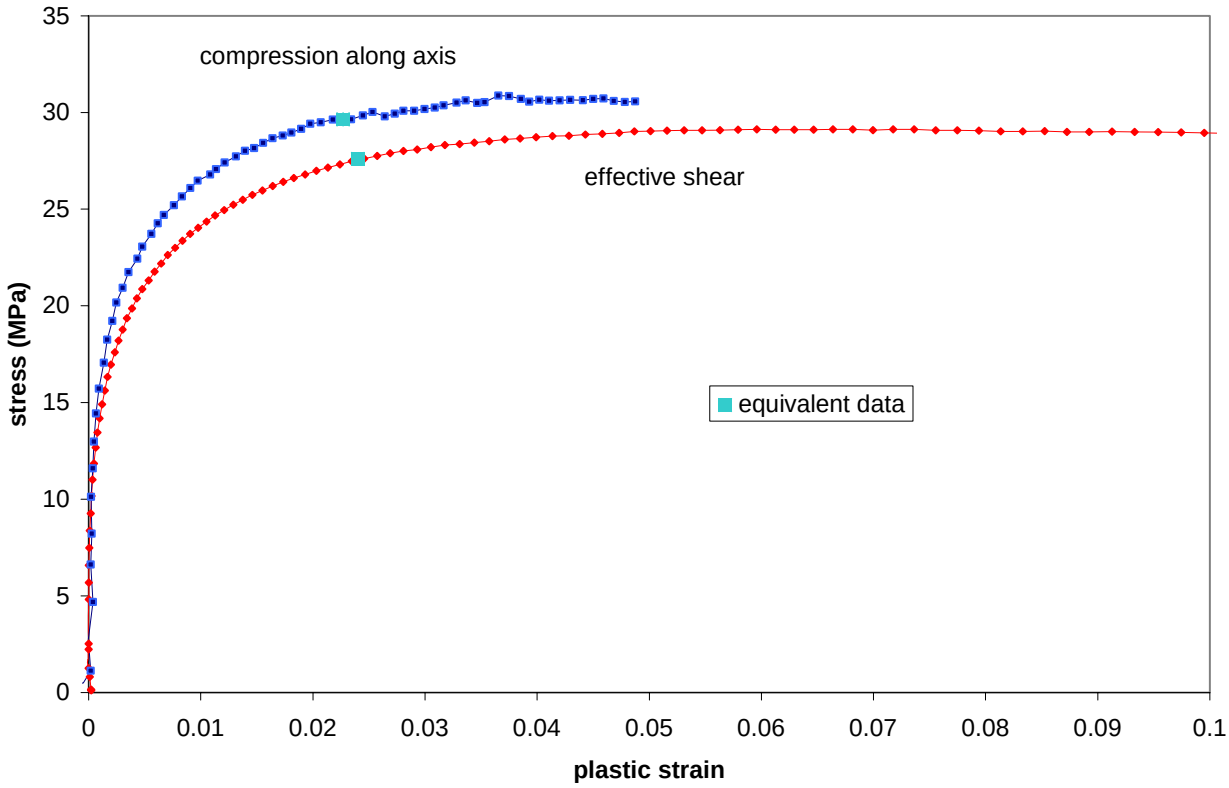

Figure 16 Hardening curves in shear and compression derived from the results in figures 9 and 5, respectively.

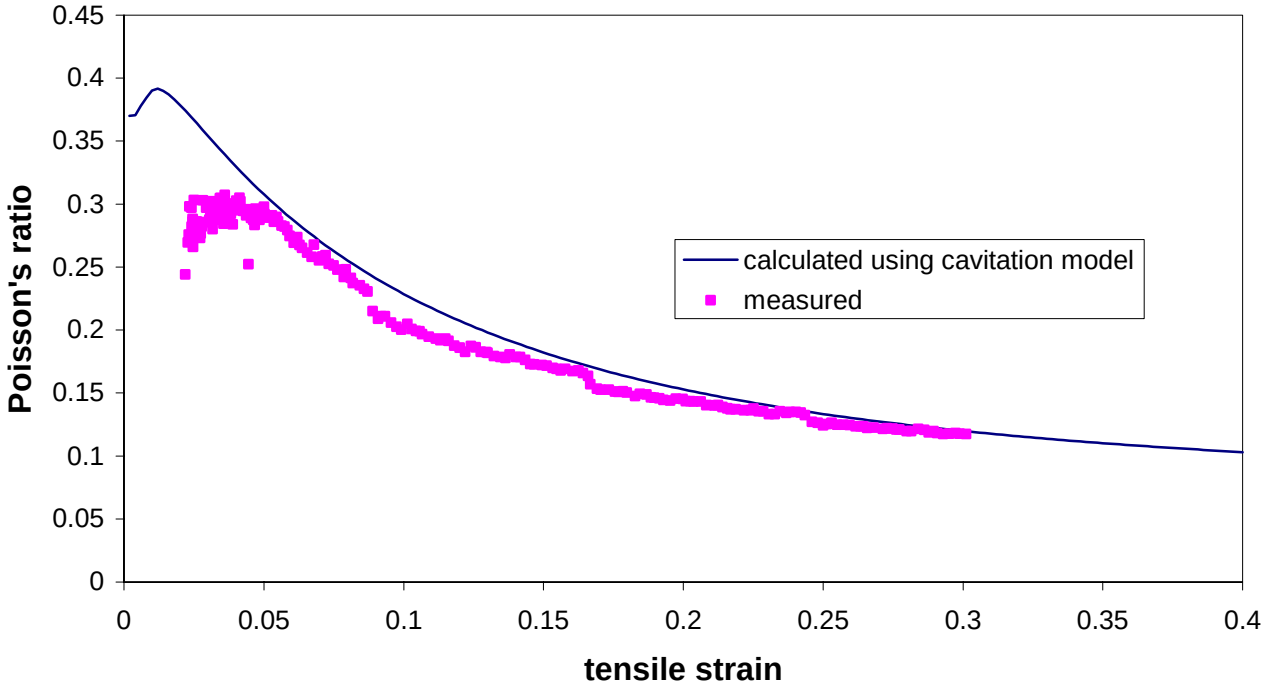

Figure 17 Comparison of measured values of Poisson's ratio with predictions using the cavitation model with a value for $v_C = 0.46$.

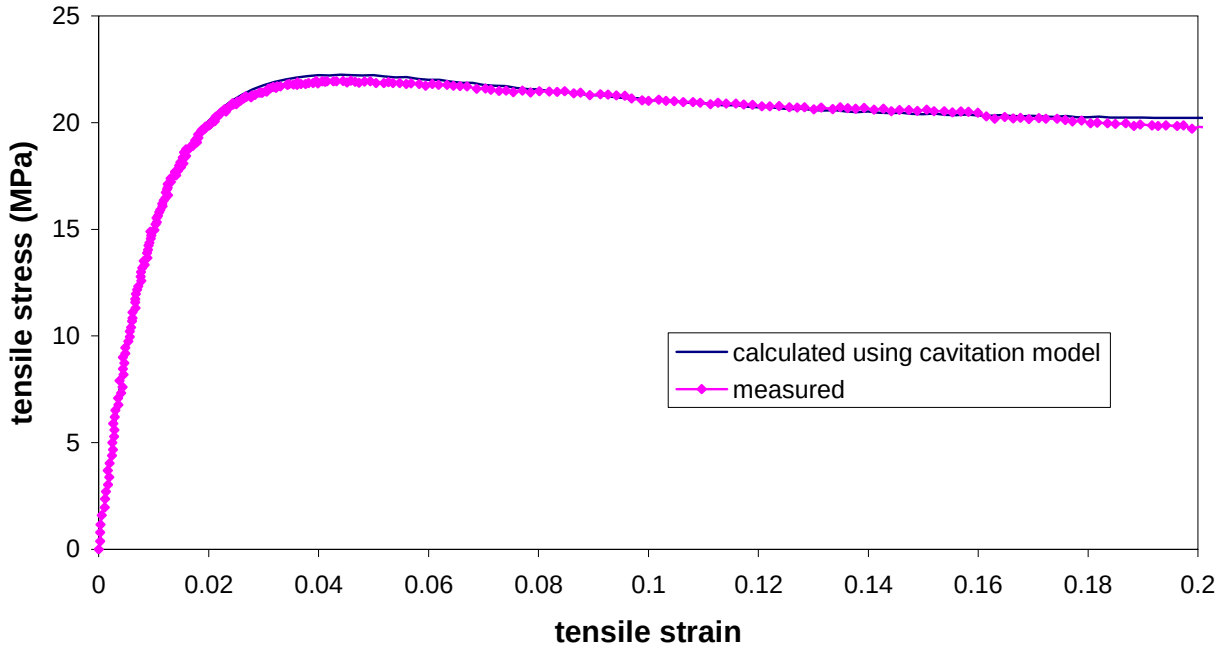

Figure 18 Comparison of measured tensile curve with predictions using the cavitation model with parameter values listed in table 2.

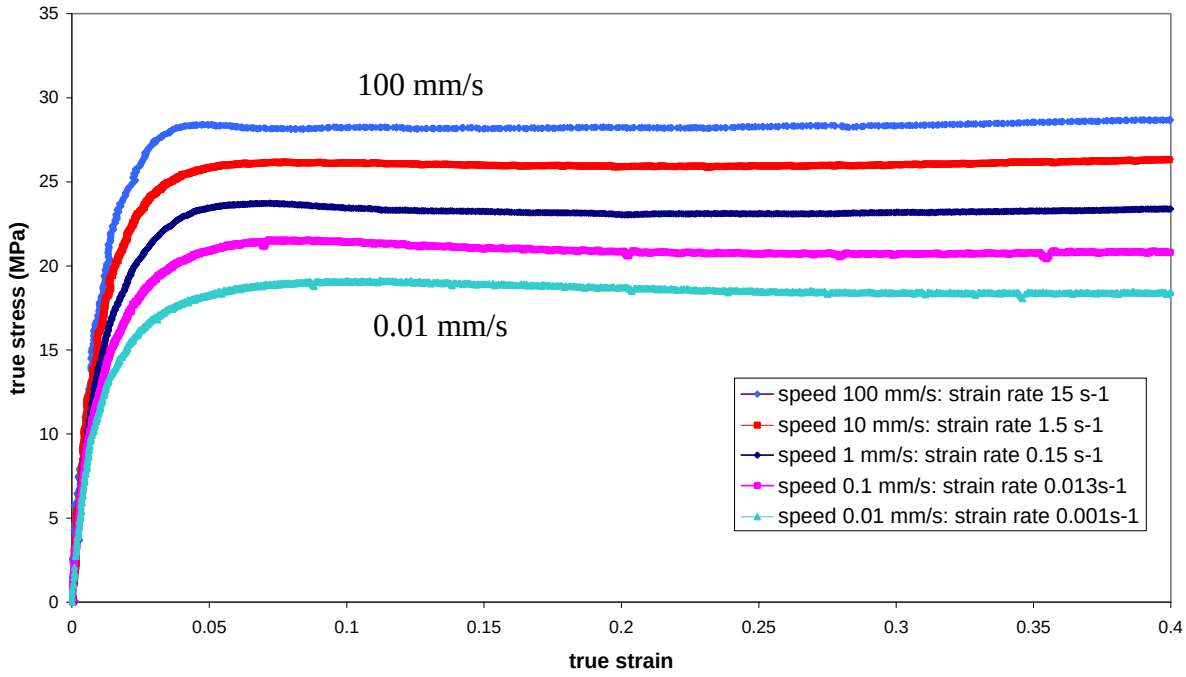

Figure 19 Tensile stress/strain curves measured on waisted injection moulded specimens at different test speeds.

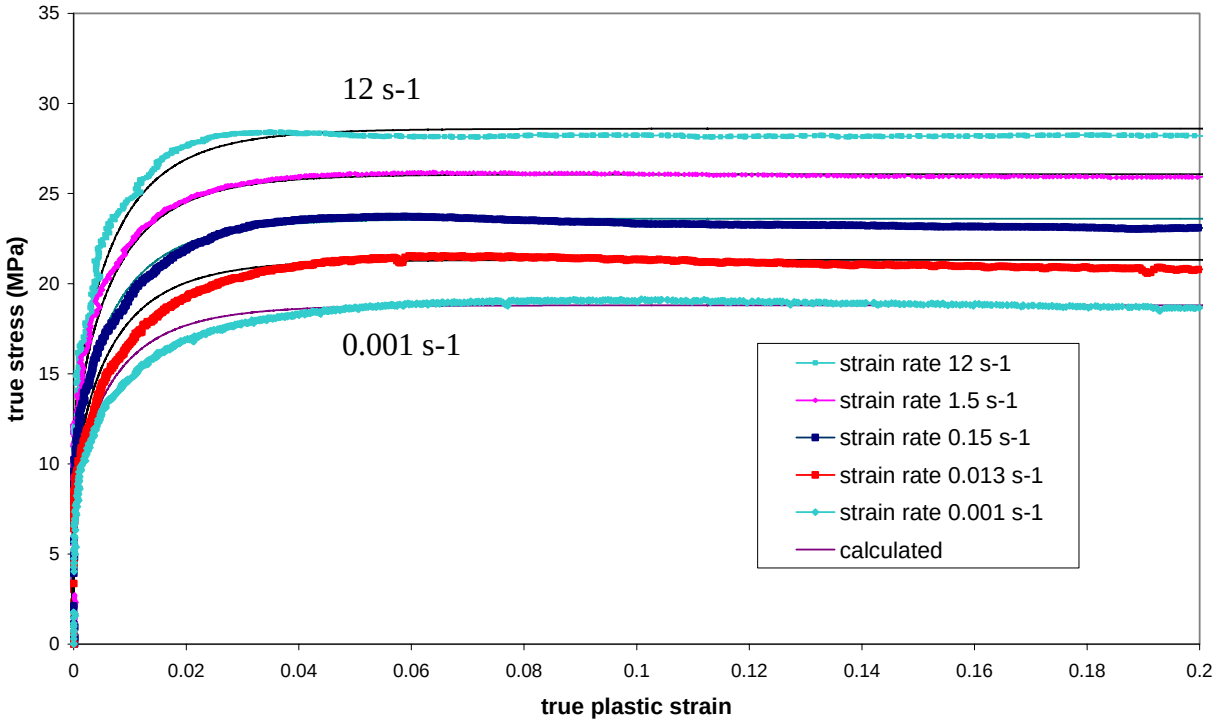

Figure 20 Hardening curves derived from the results in figure 19 and modelled using equation (29) and the parameters in table 3.

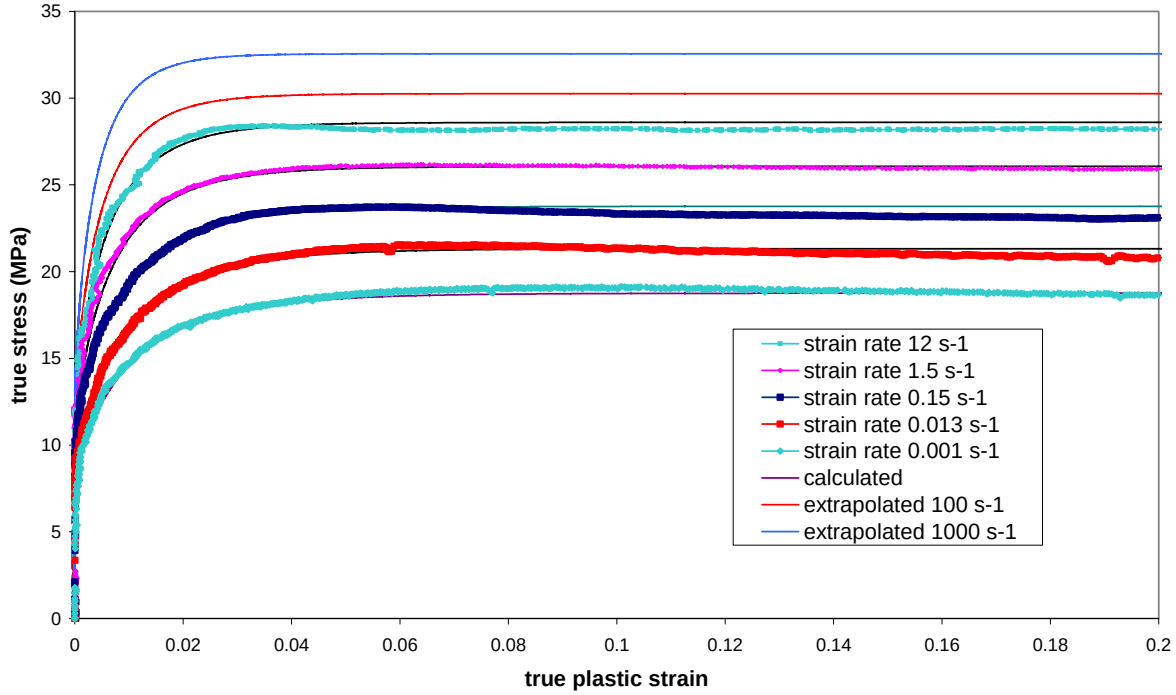

Figure 21 Hardening curves derived from the results in figure 19 and modelled using equation (29) with the parameters in table 4.

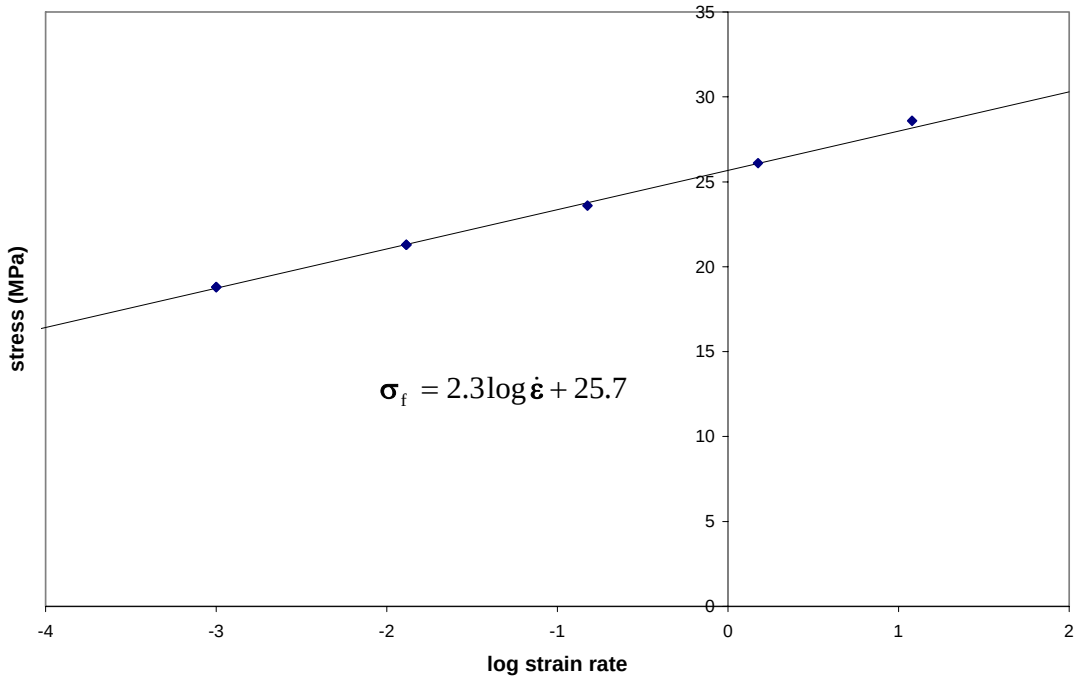

Figure 22 Plot of flow stresses σ_f in table 3 or 4 against the log of the strain rate.

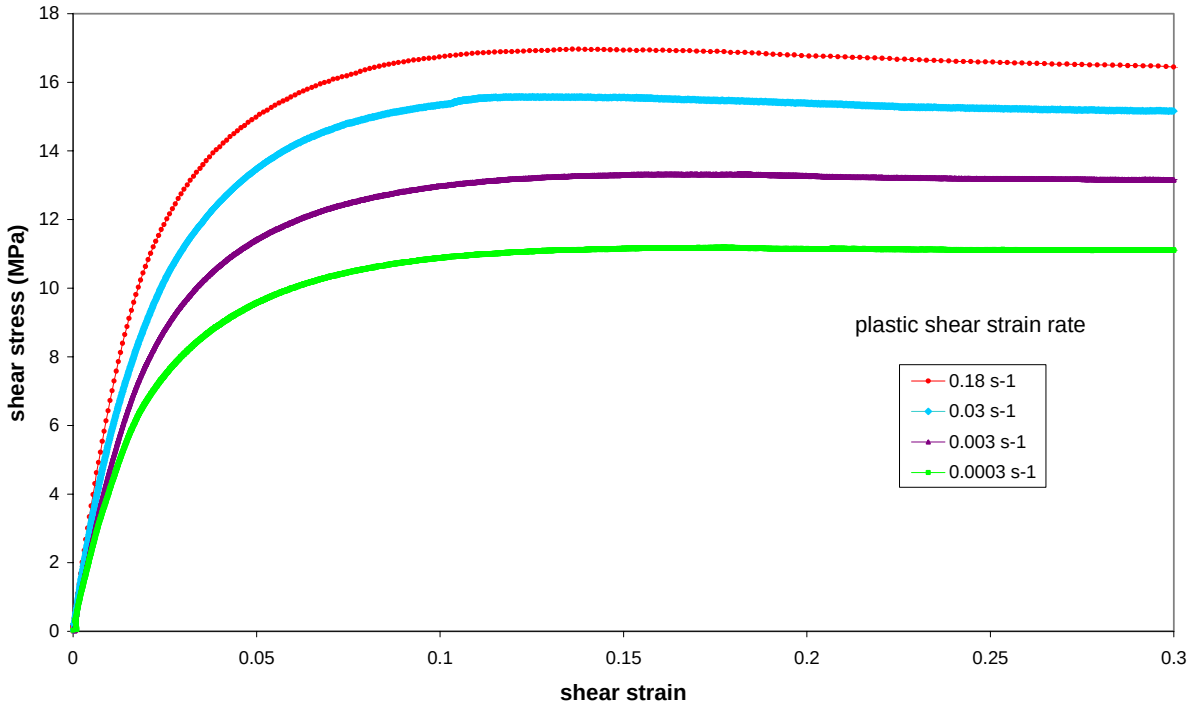

Figure 23 Shear stress/strain curves measured on injection moulded specimens at different test speeds.

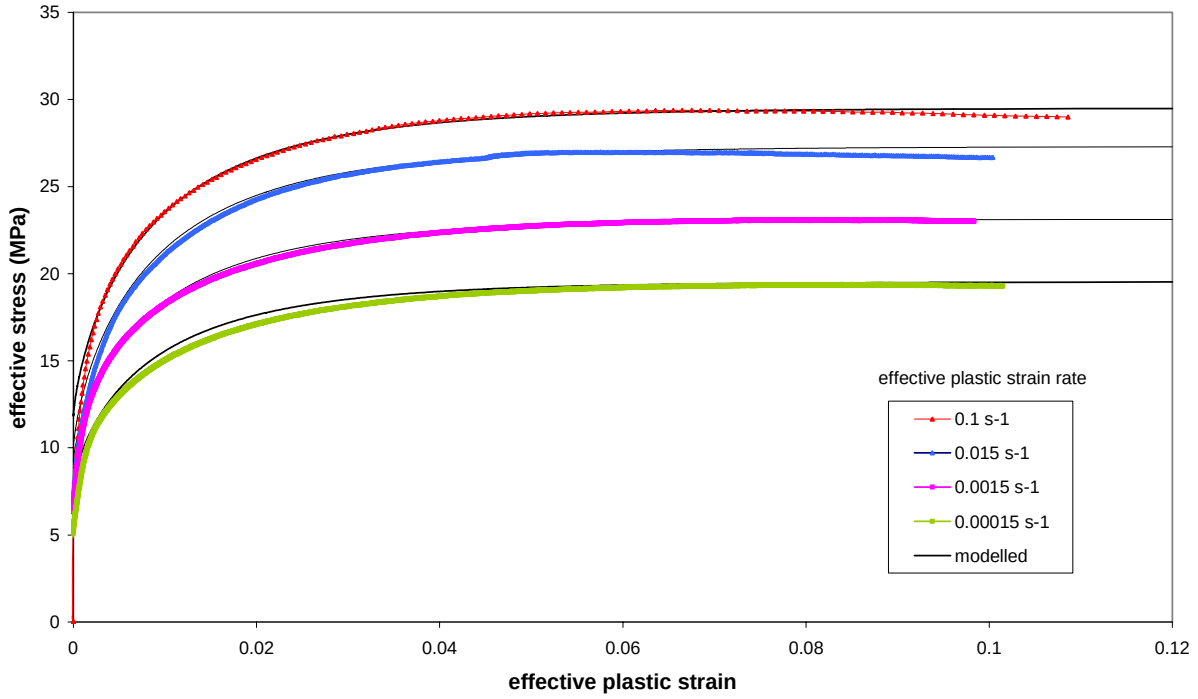

Figure 24 Shear hardening curves derived from the results in figure 23 and modelled using equation (32) with the parameters in table 5.

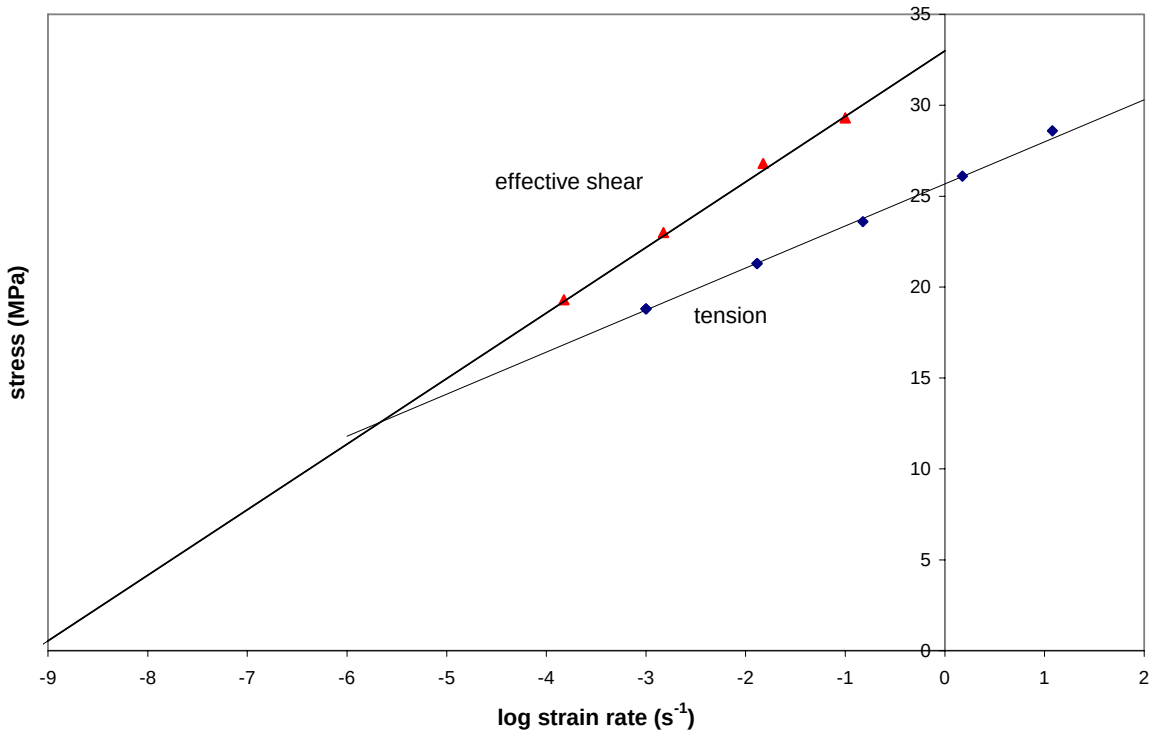

Figure 25 Comparison of plots of shear and tensile flow stresses against log strain rate for injection moulded material (see equations (30) and (33)).

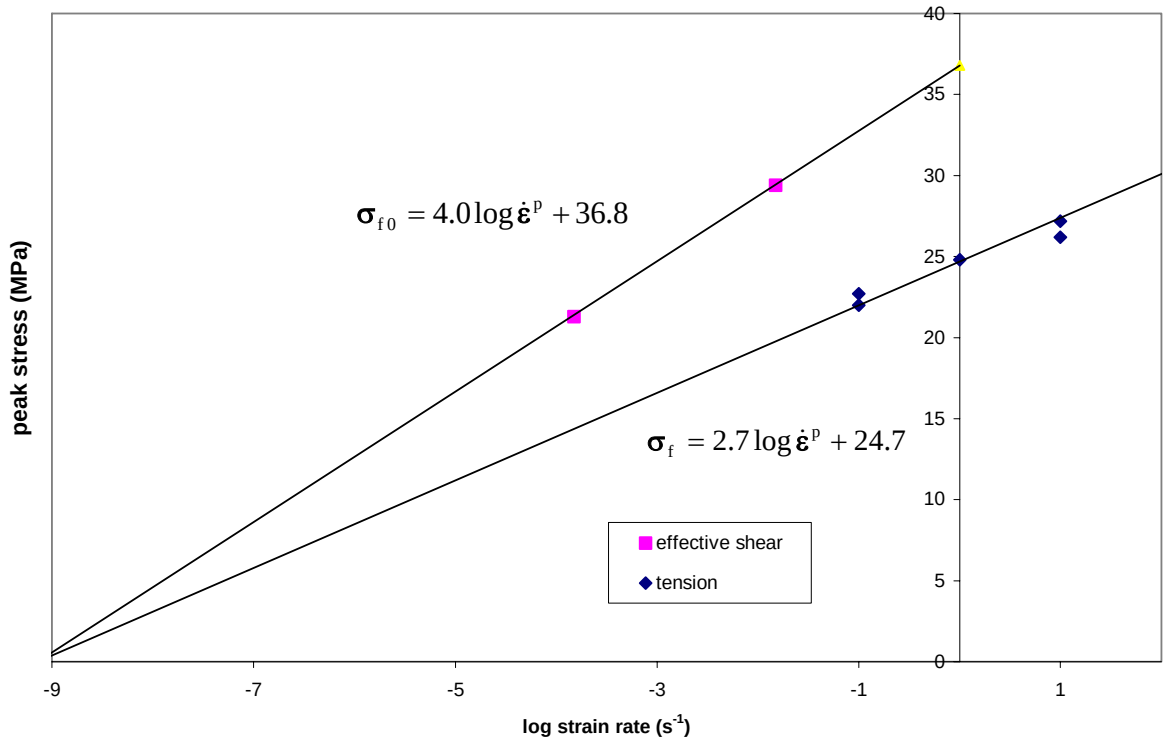

Figure 26 Eyring fits to data for the door trim material.

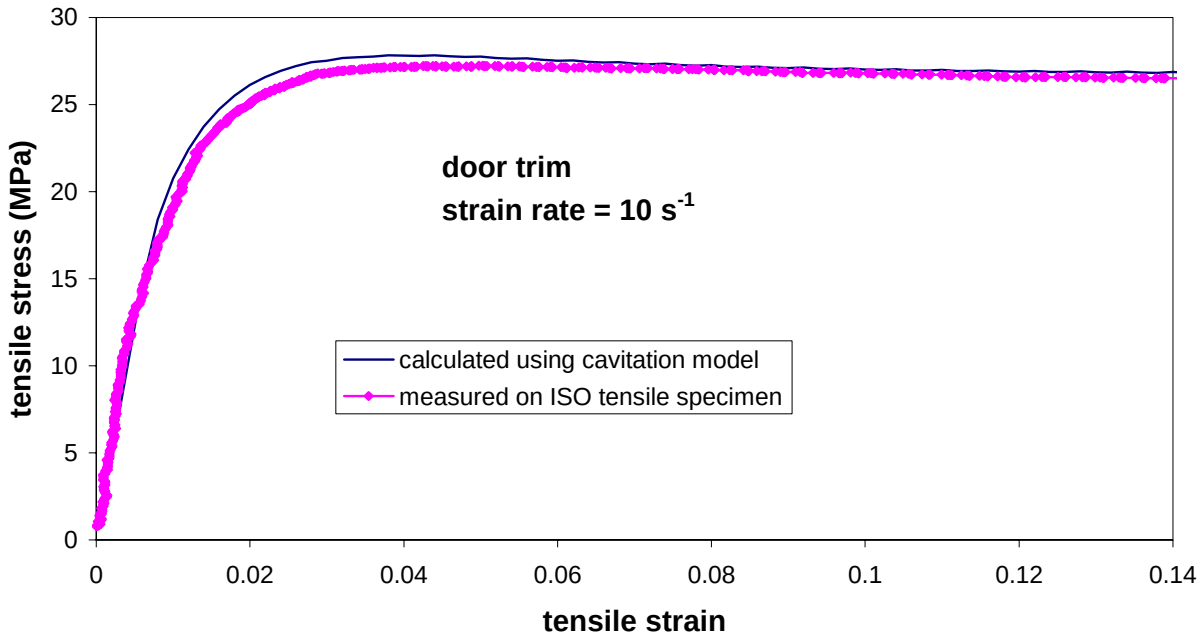

Figure 27 Comparison of the tensile stress/strain curve at a strain rate of 10 s^{-1} predicted using shear hardening data derived using equations (32) and (33) with experimental data.

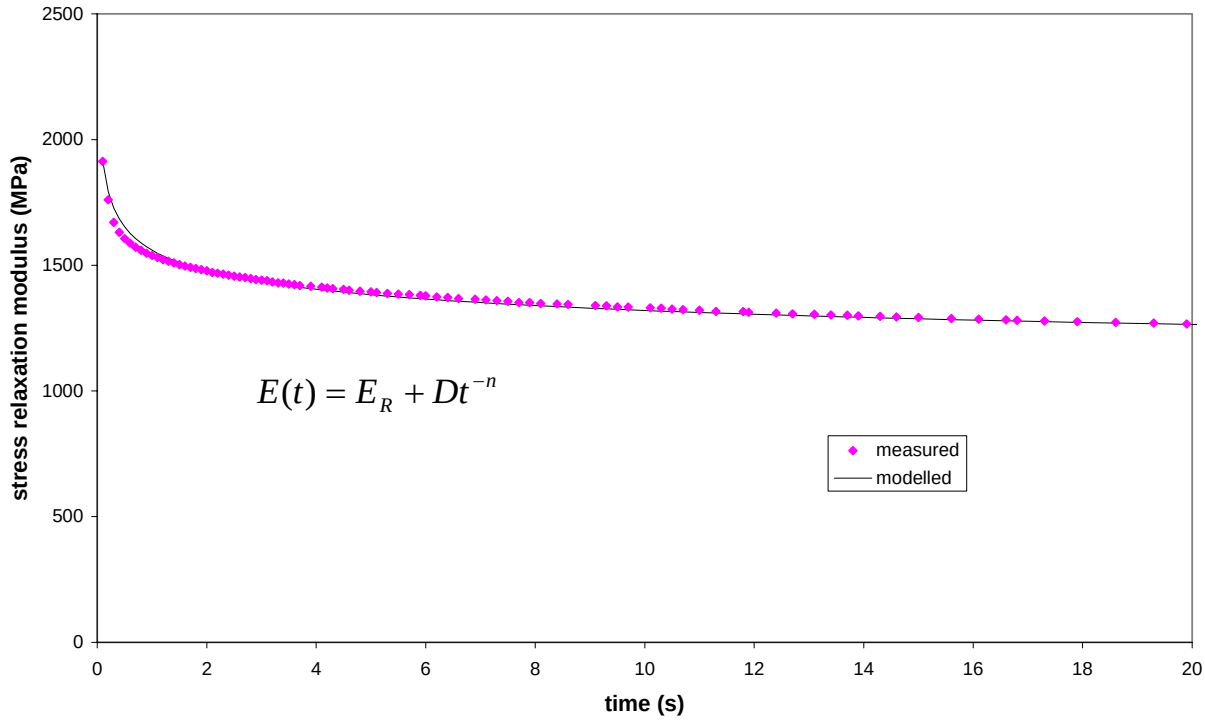

Figure 28 Stress relaxation data for an injection moulded specimen modelled using equation (38).

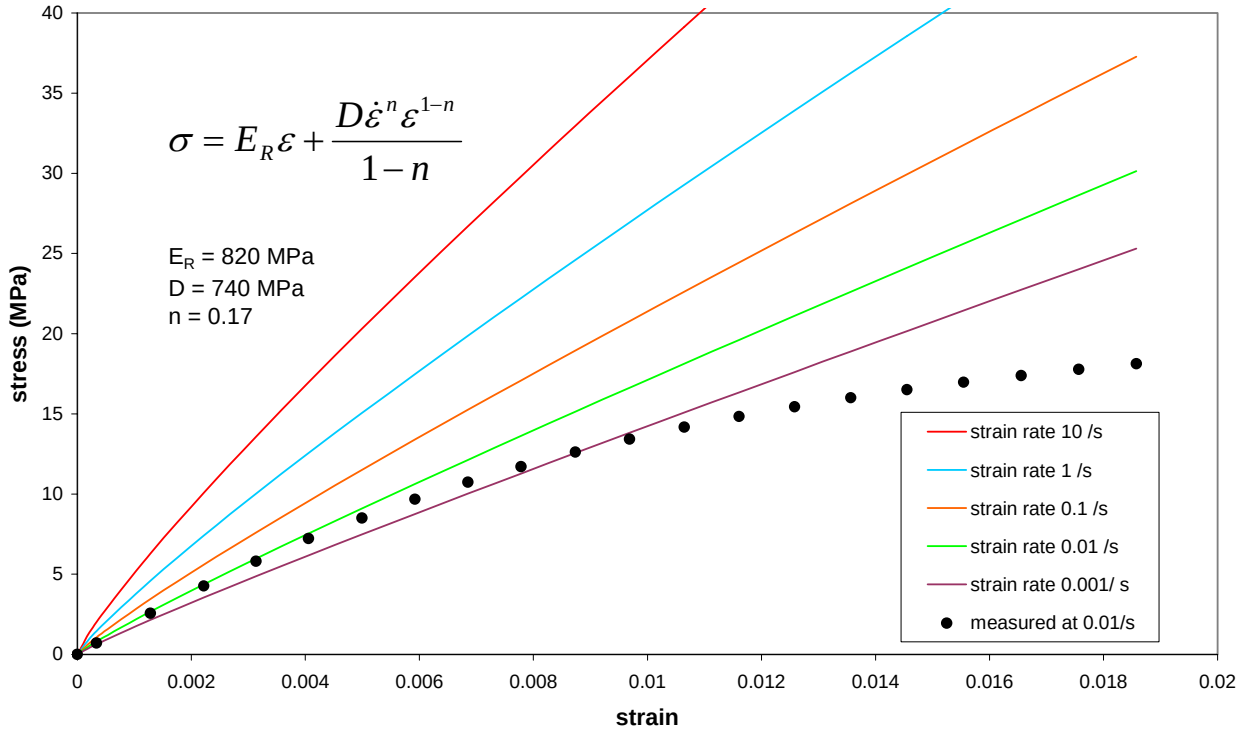

Figure 29 Stress/strain behaviour for loading at constant strain rates calculated using a linear viscoelastic analysis. The point symbols are experimental values at a strain rate of 0.01 s^{-1} and demonstrate departure from linear behaviour.